

MODELING AND SIMULATION OF SILICON PHOTONICS BASED OPTICAL RING
RESONATOR BIOSENSOR

A Dissertation in
Electrical and Computing Engineering
and
Computer Science

Presented to the Faculty of the University of
Missouri – Kansas City in partial fulfillment of the
Requirements for the degree

DOCTOR OF PHILOSOPHY

By
Liaquat Ali

Master of Science (M.S.) in Advanced Optical Technologies,
Friedrich–Alexander University Erlangen–Nurnberg, Germany, 2014

Kansas City, Missouri
2021

©2019

Liaquat Ali

ALL RIGHTS RESERVED

MODELING AND SIMULATION OF SILICON PHOTONICS BASED OPTICAL RING RESONATOR BIOSENSOR

Liaquat Ali, Candidate for the Doctor of Philosophy

University of Missouri - Kansas City, 2021

ABSTRACT

In the photonic technological platforms, the signal is carried by light rather than an electron as in conventional electronic technologies. Electronic processing of the signals is becoming restricted, particularly in the multi-GHz frequency range, due to the parasitic effects of the copper wires and other limitations of the materials used in micro and nanoelectronics domains. On the other hand, photonic technology can offer data transmission at the THz range. To harness the power of photonic technology, silicon-photonics would be a very effective platform because these devices use silicon as the optical medium that can be fabricated using the standard CMOS technology. A biosensor is an analytical device used for the identification of an analyte that conglomerates a vital element with a physicochemical indicator. Optical biosensors are comprised of a light source, light guiding medium, and photodetector. In recent decades, optical ring resonators gained importance as one of the promising biosensors due to miniaturized size and fast response. The optical ring resonator identifies the intended molecules or biochemical molecules by assessing the change in light behavior and that change in light behavior occurs due to the interactivity of the evanescent field of the resonating light with biosamples such as blood, serum, saliva, bacteria, protein or DNA traits present on the surface of the ring resonator. One of the most leading causes of death in modern times is

different types of cancer. American Cancer Society in their recent report, states that in more than 50% of death by cancer, cancer has been diagnosed at the last stage. The core target of this thesis is to outline a silicon photonics biosensor based on an optical ring resonator for the identification of cancer and other diseases.

APPROVAL PAGE

The faculty listed below, appointed by the Dean of the School of Graduate Studies have examined a thesis titled “Modeling and Simulation of Silicon Photonics based Optical Ring Resonator Biosensor” presented by Liaquat Ali, candidate for the doctorate degree, and certify that in their opinion it is worthy of acceptance.

Supervisory Committee

Masud H Chowdhury Ph.D., Committee Chair

Electrical and Computer Engineering

Yugyung Lee Ph.D., Co-Discipline Chair

Department of Computer Science Electrical Engineering

Ghulam M. Chaudhry Ph.D., Committee Member

Department of Computer Science Electrical Engineering

Cory Beard, Ph.D., Committee Member

Department of Computer Science Electrical Engineering

Ahmed M. Hassan Ph.D., Committee Member

Department of Computer Science Electrical Engineering

CONTENTS

ABSTRACT	iii
LIST OF ILLUSTRATIONS	viii
LIST OF TABLES	xi
ACKNOWLEDGEMENTS	xii
Chapter	
1. INTRODUCTION	1
Silicon Photonics Optical Biosensor Market and Applications	2
Limitation and Challenges	3
Problem Statement	3
Thesis Organization	4
2. THEORETICAL BACKGROUND	6
Single Ring Resonator Biosensor System	8
Two Ring Resonator Biosensor System	13
3. DESIGN AND MODELING	18
Grating Coupler	18
Waveguide	19
Ring Waveguide.....	23
Ring Resonator Biosensor System.....	26
4. BIOSENSOR COMPONENT OPTIMIZATION.....	28
Radii Analysis	28
Waveguide Width and Height Analysis.....	29
5. ANALYSIS OF CANCER CELL	32

Refractive Index of Cancer Cell	32
Comparison of Unoptimized and Optimized	33
6. TWO RING RESONATOR BIOSENSOR SYSTEM.....	37
Serially Coupled Two Ring Design	37
Parallel Coupled Two Ring Design	41
Cascaded Ring Resonator as a Biosensor	44
7. NON-INVASIVE REAL TIME WEARABLE ALCOHOL BIOSENSOR.....	50
Machine Learning Algorithm	51
8. CONCLUSION & FUTURE WORK.....	55
Summary	55
Future Work	56
REFERENCES	57
VITA	63

LIST OF ILLUSTRATIONS

Figure	Page
1. Block Diagram of Biosensor.....	7
2. Ring Resonator Biosensor.....	8
3. Grating Coupler for coupling optical fiber and integrated waveguide	9
4. Spectral response for all-pass ring resonator	10
5. Spectral response for add-drop ring resonator	12
6. Transmission spectrum for ring resonator circuit showing Quality factor and Extinction Ratio	13
7. Transmission Electric fields in serially coupled two-ring design[1]	14
8. Electric fields in parallel-coupled two-ring design[1]	17
9. Special parallel-coupled two-ring design [1].....	18
10. Proposed ring resonator biosensor system.....	19
11. Spectral response for grating coupler and the grating coupler circuit with multi- wavelength laser, 127 um waveguide, and photodiode	20
12. 3D modeling of an integrated waveguide in Lumerical MODE.....	21
13. Electric Field Intensity for TE01 mode propagating in waveguide.....	22
14. Energy density for TE02 mode propagating in waveguide	22
15. Magnetic Field Intensity for TE01 mode propagating in waveguide	23
16. E-field without bending and with bending of waveguide.....	24
17. (a) 3D view for the ring resonator circuit showing the through and drop port, colored part is Si and grey part is SiO2 (b)same ring resonator structure covered with known refractive index	

material and (c) Transmission spectra of ring resonator circuit at through port in Lumerical MODE.....	25
18. (a) 3D view for the ring resonator circuit with (b) Transmission spectra of ring resonator circuit through software COMSOL.....	27
19. Ring Resonator Bio Sensor System in Lumerical INTERCONNECT.....	28
20. Spectral response of ring resonator circuit for wavelength 1500 to 1600nm	28
21. Variation of (a) Sensitivity and (b) Quality factor with a change in radius of ring waveguide	30
22. Transmission spectra for different cells along with their refractive indices. Parameters for ring resonator $R = 3.1\ \mu\text{m}$, $g = 0.1\ \mu\text{m}$, $wG = 0.5\ \mu\text{m}$, $h = 0.22\ \mu\text{m}$	34
23. Transmission spectra for different cells along with their refractive indices for the optimized for ring resonator $R = 3\ \mu\text{m}$, $g = 0.1\ \mu\text{m}$, $wG = 0.45\ \mu\text{m}$, $h = 0.18\ \mu\text{m}$..	35
24. Quality factor and Sensitivity for different cancer cells for optimized ring resonator circuit.	37
25. 3D view, red color material is Si, and grey color material is SiO ₂ and (b) XY view of the serially coupled two ring resonator structure showing some parameters	39
26. (a) 3D Field Intensity and (b) Energy Density for TE ₀ mode propagating in the waveguide	40
27. Coupling of light from linear waveguide to ring waveguide at (a) 1.5924 μm (b)1.56213 μm and (c)1.5019 μm	41
28. Spectral transmission on the through port for ring resonator circuit in figure 5(a). ..	42
29. Electric Field Intensity and (b) Energy Density for TE ₀ mode propagating in the waveguide	42

30. Coupling of light from linear waveguide to ring waveguide at (a) 1.5 μm (b)1.52015 μm and (c)1.59677 μm	44
31. Spectral transmission on the through port for ring resonator circuit in figure 5(a)...	45
32. Spectral transmissions for a normal blood sample and Jurkat cell blood sample by (a) serially coupled and (b) parallel-coupled two ring resonators.....	47
33. Proposed cascaded ring resonator circuit as a biosensor for the interaction of Antibody and Antigen.....	48
34. Proposed cascaded Proposed (a) serially and (b) parallel-coupled cascaded ring resonator for the interaction of Antibody and Antigen.....	49
35. Spectral transmission after placing ant –CD3 antibody and after interaction of antigen-antibody on the surface of (a)serially and (b) parallel-coupled two ring resonator.....	50
36. Non-invasive monitoring device for asthma.....	52
37. Python code for applying different machine learning algorithms on asthma dataset.	53
38. Comparison of a different machine learning algorithm for Asthma dataset.....	53
39. The machine learning model is applied for one row of asthma dataset.....	54
40. Python for flask app for asthma monitoring	54
41. Python Flask app for Asthma severity detection.	55

LIST OF TABLES

Table	Page
1. Dimension of integrated waveguide	21
2. Different bent radius overlap with the loss for TE and TM mode.....	24
3. Ring Resonator and coupling waveguide parameters.....	26
4. Optimization of the ring resonator, radius = $3\mu\text{m}$, and gap = $0.1\ \mu\text{m}$ and changing waveguide width and height	31
5. The cancer cell line with their refractive index of the sample[2]	34
6. Resonance wavelength, quality factor, and sensitivity for normal and different cancer blood sample from optimized ring resonator	36
7. Comparison with other work	37
8. Refractive index of healthy blood and leukemia blood	46
9. Quality factor and sensitivity for cascaded configuration	46

ACKNOWLEDGEMENTS

Foremost, I would like to express my sincere gratitude to my advisor Prof. Masud H Chowdhury for the continuous support of my Ph.D. study and research, for his patience, motivation, enthusiasm, and immense knowledge. His guidance helped me in all the time of research and writing of this thesis. I could not have imagined having a better advisor and mentor for my Ph.D. study.

Besides my advisor, I would like to thank the rest of my thesis committee: Prof. Yugyung Lee, Prof. Ghulam Chaudhry, Prof. Ahmed Hassan, and Prof. Cory Beard, for their encouragement and insightful comments.

I thank my fellow lab mates in Micro & Nano-electronics Lab Group: Abdul Hamid B. Yousuf, Marouf Khan, Moqbull Hossain, Mahmood Uddin Mahmood, and Farid Ahmed, for the stimulating discussions, for the long days we were working together before deadlines, and for all the fun we have had in the last four years.

I would also like to thank my family: my mother Masooma Qadam Ali and late father Qadam Ali Akhter, for giving birth to me in the first place and supporting me spiritually throughout my life. Last but not the least, I would like to thank my wife, Amna Batool and my daughter, Ifrah Fatima Ali for giving me the strength and meaning to complete my Ph.D.

CHAPTER 1

INTRODUCTION

Human physical health and fitness are very important human essential. People spend their valuable time and money behind it. The techniques to monitor and inspect human health depend on the sensors which analyze the interactions of human body cells with another transducing device. These sensors are called biosensor, which is an analytical device used for the identification of an analyte that conglomerates a vital element with a physicochemical indicator [3]. These devices do those tasks and recover even more information about the diseases by the analysis of the molecule's interactions with the help of the computer. Biosensors were introduced in the 1960s by the pioneers like Clark and Lyons [4]. There are numerous types of biosensors namely enzyme-based, tissue-based, magnetostrictive, and piezoelectric biosensors, etc. These devices cater to the specific interaction between a bio molecule which could be enzyme, antigen, or nucleic acid, and the analyte of interest. The biomolecular interaction is then transduced into a recognizable signal which is readable and quantifiable. Biosensors are categorized depending on the nature of the transduction mechanism, namely as mechanical, electrical, or optical. This thesis presents the design and modeling of an innovative optical biosensor system based on silicon photonics technology, which enables high sensitivity, high-quality factor, fast response, and low-cost design.

In the photonic technological platforms, the signal is carried by light rather than an electron as in conventional electronic technologies [5]. Electronic processing of the signals is becoming restricted, particularly in the multi-GHz frequency range, due to the parasitic effects of the copper wires and other limitations of the materials used in micro and nanoelectronics domains. On the other hand, photonic technology can offer data transmission at the THz

range[6]. To harness the power of photonic technology silicon-photonics would be a very effective platform because these devices use silicon as the optical medium that can be fabricated using the standard CMOS technology [7]. The incorporation of a very high index contrast (and thus substantial miniaturization) and the availability of CMOS fabrication technology are enabling the utilization of matured electronics fabrication facilities to make photonic circuitry. As a result, silicon-photonics has been established as the leading technology for the integration of photonics and electronics in the same application systems [7].

1.1 Silicon Photonics Optical Biosensor Market and Applications

In recent decades, optical ring resonators gained importance as one of the promising biosensors due to miniaturized size and fast response. The applications of these optical sensors are mostly in the clinical sector[8], but they are also popular in the food industry[9], environmental and toxic detection[10], memory design[11]-[12], defense and marine applications[13]. While Silicon photonics has also been widely used in optical fiber communication, optical modulators, optical detection, and optical sensing applications [14], [15]. Among various types of silicon photonic biosensors, the most common are photonic crystals [16], disk resonators [17], Bragg gratings [18], strip waveguide [19], and waveguide ring resonators [17-18]. The technology of optical biosensors attains more importance due to the incorporation of silicon photonics. As silicon photonics integrated circuits use the already matured CMOS foundry technology. In grand view research report it says that the optical biosensors market was esteemed at \$17,500.0 million in 2018 and is anticipated to gain \$38,600.2 million by 2026, recording a CAGR of 10.4% from 2019 to 2026, while the Yole Development report states that the silicon technology market will grow from \$480 million to \$3.9 billion in the year 2025.

1.2 Limitation and challenges

There has been tremendous research in the last few decades about biosensors in general and in particular last decade wonderful innovation has been done in optical biosensors. But it would take at least three decades more for these biosensors to be used as a general commercial product. Current biosensors used in the commercial market for diagnostic and prognosis are comprised of biosensors other than optical although some of them are reliable, they require a significant amount of time for detection. These biosensors are very expensive to fabricate and they require someone with excellent knowledge to use those sensors for monitoring health conditions. The optical biosensors which are currently being in the research domain are fabricated in specialized laboratory facilities and it would take a very long time to convert that specialized laboratory into a commercial manufacturing product. Even after research is performed to fabricate a silicon photonics biosensor system, there are no external quality control and laboratory accreditation systems to endorse the clinical trials and results for the commercialization of biosensors.

1.3 Problem Statement

This thesis presents the modeling and design of optical ring resonator biosensors based on silicon photonics technology for cancer detection. The second-largest disease all over the world with an increasing death rate over the past few years is cancer, for which over 200 types have been identified. Breast cancer is one of the three most common invasive cancers highly widespread in females and reckons for the second-highest number of deaths worldwide. Despite the recent scientific and technical development, the survival rate of cancer patients is still weak because of detection at the later stage and the poor prognosis of cancer. A recent study by the American Cancer Society shows that an estimated 50% of all cancer death in the US are diagnosed at a later stage[21]. Whereas if these cancers could be detected at an early

stage, then more effective treatment and prevention could be applied. Burdensome, expensive, and time-consuming diagnosis methods presently available for the detection of breast cancer raise the need for the origination of unique, unconventional, and highly sensitive devices. This research project aims to the first plan, design, simulate, develop, and then test a silicon photonics optical ring resonator biosensor for detection, prognosis, and therapy monitoring for blood-based biomarkers in breast cancer. The biosensor system would have a faster response time and would be less expensive as compared to current commercial biosensor use for cancer detection.

1.4 Thesis Organization

The main objective of this thesis is to investigate, design, model and simulate silicon photonics optical ring resonators for bio sensing application. First, different components of the biosensor are modeled, and after they are combined in the shape of a system to simulate by finite domain time-domain method using Lumerical software. Several potential component optimization solutions and optimization on complete biosensor systems are discussed as well. The thesis begins in Chapter 2 with a theory and literature survey and theory of different types of optical resonators, types of ring resonator integrated circuits, and parameters to quantify ring resonator circuit and end with theory for two ring resonators namely series and parallel. Chapter 3 discuss the modeling of the main components of the proposed biosensor design separately and reasons for selecting the parameters for each component. Chapter 4 presents the analysis for detecting the different cancer cells by the proposed biosensor system. Chapter 5 shows the design and modeling for cascaded ring resonators in series and parallel fashion. Chapter 6 discuss the disease asthma and how machine learning algorithm can be applied to detect the asthma attack. The final chapter 7 present the summary of the main findings and

conclusion of the thesis and a dialog of possible future work.

CHAPTER 2

THEORETICAL BACKGROUND

In this chapter, we will discuss the theoretical background of ring resonator biosensors. Each component of the ring resonator would be present and at the end of the chapter, the theory of the two ring resonator will be discussed. A biosensor is an analytical device, streaked for the identification of an analyte that conglomerates a biological element with a physicochemical indicator [3] as shown in Figure 1. The biosensor was started in the 1960s by the pioneers Clark and Lyons [4]. There are numerous types of biosensor namely enzyme-based, tissue-based, magnetostrictive, and piezoelectric biosensors, etc. the application of these sensors are mostly in the clinical sector, but they are popular in the food industry, environmental and toxic detection, defense, and marine applications. In an electrical biosensor the identification of biological analyte is transformed into an electrical signal so apparently by detecting; the change in the electrical signal bio reaction can be detected. Whereas the optical biosensors, the recognition of biological analyte is transformed into some relative properties of light. Optical biosensors are comprised of the light source, light guiding medium, and photodetector. In recent decades, optical ring resonators gained importance as one of the propitious biosensors due to miniaturized size and fast response. The optical ring resonator identifies the intended molecules or biochemical molecules by assessing the change in light behavior and that change in light behavior occurs due to the interactivity of the evanescent field of the resonating light with bio samples such as blood, serum, saliva, bacteria, protein or DNA samples present on the surface of the ring resonator. In response to that interactivity in the medium changes the combined or effective refractive index of the bounded bio sample, which reciprocates in a change of the resonance wavelength of the resonator.

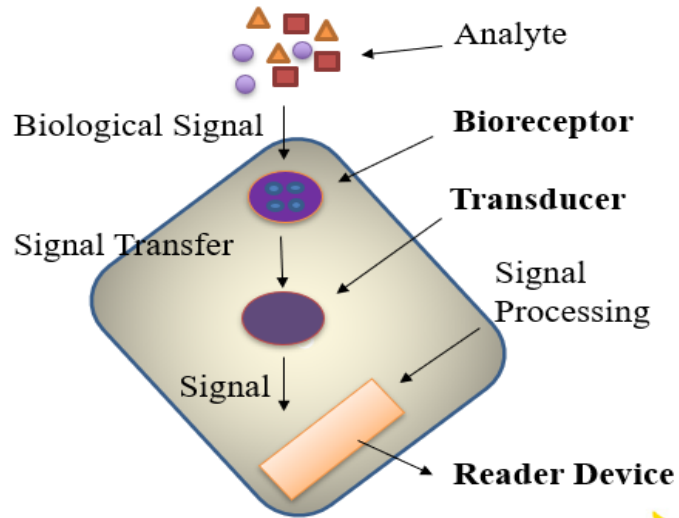


Figure 1 Block Diagram of Biosensor

The change of resonance wavelength is related to several bio molecules in the bio sample[22]. There are many categories of silicon photonic biosensors namely photonic crystals [16], disk resonators [17], Bragg gratings [18], strip waveguide[19], and waveguide ring resonators [20] based on the same principle in which the change in refractive index is transferred into a change in resonance wavelength.

In general, ring resonators can be design and developed in two models [23]. In the first model, two optical fibers are used, one to develop a ring by connecting two ends of fibers and the second optical fiber to couple the optical light into the ring [24]. The second model is integrated optical structures (by integrated optics technology). These optical structures are more consistent and replicate multiple times. They also offer multiple detections of bio particles at the same time by fabrication of similar ring resonators on a single chip and covering the surface of the ring resonator with a different layer[14], [20-21].

One of the most leading causes of death in modern times is different types of cancer. American Cancer Society in their recent report [22] states that in more than half of death by cancer, cancer has been diagnosed at the last stage. The report statistically proves that

these cancer deaths could be prevented if cancer could be detected at the initial stages. Currently, the techniques, which could detect cancer at an early stage, are very limited in sensitivity and resolution [27]. The core target of this paper is to outline a silicon photonics biosensor based on an optical ring resonator to be used for the detection of cancer cells.

2.1 Single Ring Resonator Biosensor System

The overall system for biosensors consists of multi-wavelength laser, optical fiber, grating couplers, waveguides, ring resonator waveguide, coupling waveguide, and photodetector as shown in Figure 2.

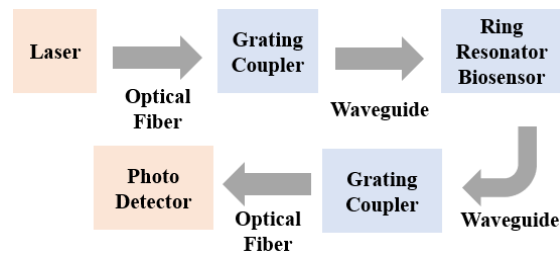


Figure 2: Ring Resonator Biosensor System

Grating Coupler

It is tough to couple optical light from a laser to an integrated waveguide. This is because the typical radius of an optical fiber is around 125um whereas in the integrated waveguide the core layer, where the guided mode is enclosed of has a width in the range of 100-300nm. A grating coupler as shown in Figure 3. is used as a coupler between the optical fiber and integrated waveguide. To address this coupling problem several groups have recently demonstrated coupling losses below 1 dB using an inverted lateral taper with a polymer overlay [28]-[29]. surface coupling is one solution for the coupling problem, which allows that coupling can be performed at any place of the chip a shown in Figure 3.

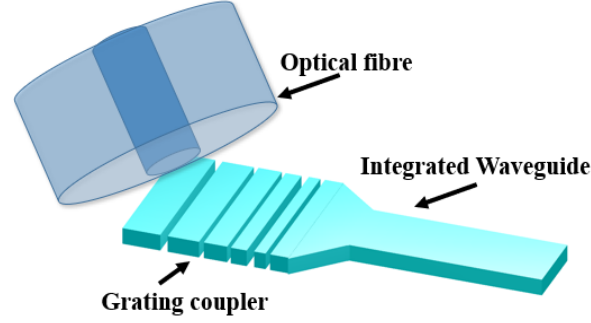


Figure 3: Grating Coupler for coupling optical fiber and integrated waveguide

Optical Ring Resonator

One of the ways to make an optical ring resonator is to combine the two ends of a single wave guide and forms a ring structure. The ring structure will trap the optical light inside and the light will resonant after constructive interference at the resonance wavelength. The process of the resonance of an electromagnetic wave can be described mathematically as (1).

$$kd = 2\pi m \quad (1)$$

where $k = nk_0$ is the wave number of the light, d is the distance covered by the optical light in round trip and m is the resonance mode. In optical ring resonator, d could be exchanged with the parameter of the ring as $k = 2\pi n_{eff} / \lambda_0$, in which n_{eff} is the effective refractive index and λ_0 is the resonance wavelength. Applying the aforesaid modifications to equation (1), the resonance wavelength would be

$$\lambda_0 = \frac{2\pi n_{eff} R}{m} \quad (2)$$

where R is the radius of the ring. Equation (2) shows the directly proportional relationship between the effective refractive index and resonance wavelength.

Optical ring resonators can be clustered into two main categories depending on the number of couplers that are present along the ring resonator. The first type, the All-pass filter

has one coupler whereas the second add-drop filter has two couplers along with the ring structure. Both types of optical ring resonators are defined comprehensively in [30].

All-Pass Filter

The structure shown in with one linear waveguide and a ring is an all-pass optical filter, where the linear waveguide is used to couple optical light into ring waveguide. The same waveguide is used as an input and output port. The output port usually is named the Through port. The optical light inserted into the input port transmits through the waveguide to reach the coupling region, which is the area of the waveguide with the minimum distance from the ring resonator. In this area, a part of the light evanescently couples to the ring.

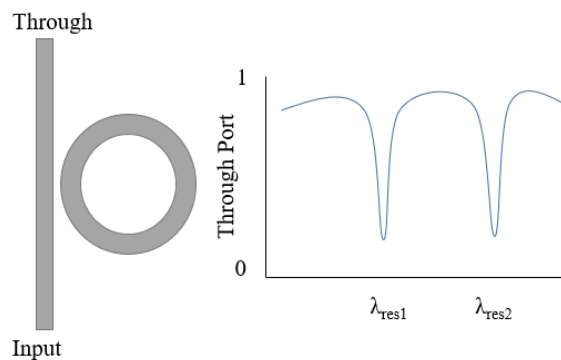


Figure 4 Spectral response for all-pass ring resonator

The amount of coupling depends on the gap or the spacing between the waveguide and the ring, the dimension of the ring waveguide which will define the matching of propagation constant of mode propagating inside the linear waveguide and resonating mode in the ring. At resonance wavelength, the light will trap and build up the energy, whereas at the other wavelength optical light transmits through the linear waveguide to output without coupling to the ring waveguide. The transmission response all-pass filter is expressed by the following equation.

$$T_{AP} = \frac{a^2 - 2racos\varphi + r^2}{1 - 2racos\varphi + (ar)^2} \quad (3)$$

where φ is a phase shift of the light after one round-trip inside the ring, a is the amount of diminution of light after one round-trip, and r is the self-coupling coefficient of the coupler.

Add-drop Filter

In the add-drop configuration, two linear waveguides are positioned on each side of the ring waveguide as shown in figure 5 with its spectral response. The first waveguide is to insert the optical light into the ring resonator and the second waveguide is to couple the optical lights out of the ring resonator. In this structure, there are four ports, the input port and through the port which is similar to an all-pass filter. Drop port has the output which is reciprocal of the through the port with some losses and add port is used to introduce any specific wavelength optical light. The transmission response for the add-drop filter is expressed by the following equation[31]

$$T_{Through} = \frac{a^2r_2^2 - 2r_1r_2acos\varphi + r_1^2}{1 - 2r_1r_2acos\varphi + (ar_1r_2)^2} \quad (4)$$

$$T_{Drop} = \frac{a^2r_2^2 - 2r_1r_2acos\varphi + r_1^2}{1 - 2r_1r_2acos\varphi + (ar_1r_2)^2} \quad (5)$$

where r_1 and r_2 are self-coupling coefficients of the first and second couplers, respectively.

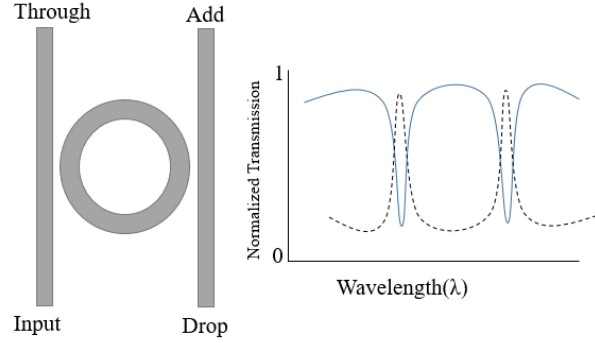


Figure 5 Spectral response for add-drop ring resonator

The properties sensitivity, quality factor, extinction ratio, and free spectral range are few parameters to characterize the optical ring resonator. The sensitivity(S) for the ring resonator is the ratio of change in the resonant wavelength due to a change in refractive index. Sensitivity is to be measured in terms of nm/RIU and it should be high as possible.

$$S = \frac{\Delta\lambda}{\Delta n} \quad (6)$$

where $\Delta\lambda$ is the change in resonant wavelength and Δn is the change in refractive index. The quality factor (Q) is defined as the ratio of resonant wavelength to change in the wavelength at Full Width Half Maximum (FWHM). The quality factor should be as high as possible and it is a unit-less parameter.

$$Q = \frac{\lambda(\text{resonant})}{\Delta\lambda(\text{FWHM})} \quad (7)$$

where $\lambda(\text{resonant})$ is the wavelength at resonance and $\Delta\lambda(\text{FWHM})$ is the difference of wavelengths obtained at FWHM. The extinction ratio for the ring resonator is defined as the ratio of the maximum amplitude to the lowest amplitude on a logarithmic scale.

$$ER = 10\log_{10}(P_L/P_H) \quad (8)$$

where P_L is minimum amplitude and P_H is the maximum amplitude of the signal at the resonance wavelength through the port. Free spectral range (FSR) is defined as the spacing in

optical frequency or wavelength between two successive reflected or transmitted optical lights at maximum or minimum amplitude. All these said properties are shown in figure 6 for the typical spectral response of the ring resonator.

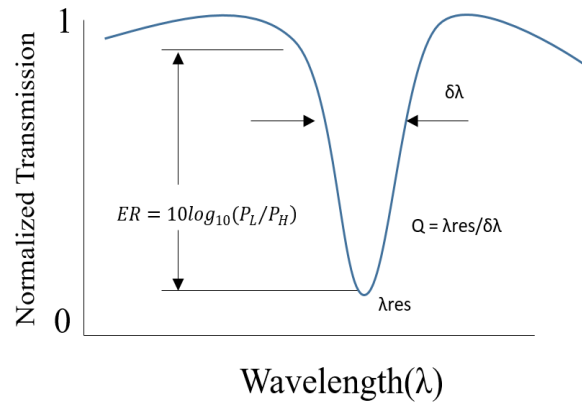


Figure 6 Transmission spectrum for ring resonator circuit showing Quality factor and Extinction Ratio.

2.2 Two Ring Resonator Biosensor System

The two-ring resonator system is widely applied in telecommunication systems as a closed filter. As of the characterization viewpoint, in the two-ring structure configured in series, the input port and the drop port will have the same direction, so that many devices can be connected easily. The parallel and series structure has been presented in [32]-[33]. In the series configuration, the rings are placed vertically on top of each other in such a way that signal from the bottom of one ring is sequentially passed through to the other ring. Due to this power transfer, all the rings in the structure must have the same resonant wavelength. The gap between the two rings obtains the combined resonant line shape in the series structure. In the parallel design, both the rings are coupled to the input and drop port waveguide. In this design, the rings can be combined to one another giving a wavelength selective reflector as presented

in [34]. The rings are interconnected in such a way that the same optical light from the input waveguide port is coupled to both ring resonators simultaneously. Due to that, in this design, the resonance wavelength for both ring resonators is not compulsory. The length of the waveguide defines the resonant line shapes. There will be several peaks or dips in these designs, which convert into nonaligned resonant frequencies. In the later section, we present the transfer function for the two-ring resonator configured in a serial and parallel configuration.

Serially Coupled Two Ring Design

The representation of a serially coupled two-ring design is shown in figure 7 From the geometric modeling and applying the methods in [1], the electric fields presented in figure 7 can be analyzed as follows:

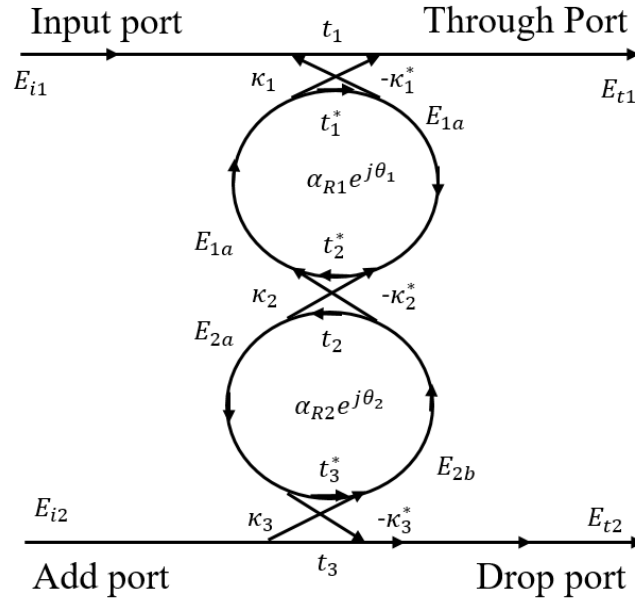


Figure 7 Transmission Electric fields in serially coupled two-ring design [1]

$$E_{1a} = -k_1^* E_{i1} + t_1^* \alpha_1 e^{j\frac{\theta_1}{2}} E_{1b} \quad (2)$$

$$E_{1b} = t_2^* \alpha_1 e^{j\frac{\theta_1}{2}} E_{1a} - k_2^* \alpha_2 e^{j\frac{\theta_1}{2}} E_{2b} \quad (3)$$

$$E_{2a} = k_2 \alpha_1 e^{j\frac{\theta_2}{2}} E_{1a} + t_2 \alpha_2 e^{j\frac{\theta_2}{2}} E_{2b} \quad (4)$$

$$E_{2b} = -k_3^* E_{i2} + t_3^* \alpha_2 e^{j\frac{\theta_2}{2}} E_{2a} \quad (5)$$

$$E_{t1} = t_1 E_{i1} + k_1 \alpha_1 e^{j\frac{\theta_1}{2}} E_{1b} \quad (6)$$

$$E_{t2} = t_3 E_{i2} + k_3 \alpha_2 e^{j\frac{\theta_2}{2}} E_{2a} \quad (7)$$

where $\alpha_{1,2} = \alpha_{R1_{1/2}}, \alpha_{R2_{1/2}}$ represents the half round trip loss coefficients of ring resonators one and two, respectively. From (2) to (7), the general expressions for the transfer functions for the throughput and the drop port can be derived. A simplified form can be obtained by assuming a coupler without losses and symmetric coupling behavior, setting $t = t^*$ and $\kappa = -t^*$ (note that the phase factor $-j$ has not been introduced into the assumption and can be added if required) which gives the ready to use amplitude forms for the throughput port ($E_{i2} = 0$).

$$\frac{E_{t1}}{E_{i1}} = \frac{-t_1 \kappa_1^2 \alpha_1 e^{j\theta_1} (t_3 \alpha_2 e^{j\theta_2} - t_2)}{1 - t_3 t_2 \alpha_2 e^{j\theta_2} - t_2 t_1 \alpha_1 e^{j\theta_1} + t_3 t_1 \alpha_1 \alpha_2 e^{j\theta_2} e^{j\theta_2}} \quad (8)$$

and for the drop port:

$$\frac{E_{t2}}{E_{i1}} = \frac{\kappa_3 \kappa_2 \kappa_1 \alpha_1 \alpha_2 e^{j\frac{\theta_1}{2}} e^{j\frac{\theta_2}{2}}}{1 - t_3 t_2 \alpha_2 e^{j\theta_2} - t_2 t_1 \alpha_1 e^{j\theta_1} + t_3 t_1 \alpha_1 \alpha_2 e^{j\theta_2} e^{j\theta_2}} \quad (9)$$

Firstly the ring coupling coefficient $\kappa_1(\kappa_3)\kappa_1(\kappa_3)$ is calculated, and secondly, it is assumed that $\kappa_1 = \kappa_3$ for the simplicity of the model. The appropriate coupling values are computed, applying the index profile and geometry in [33] and [35]. The FSR can be made larger by changing the radius of one ring resonator ($R_1 \neq R_2$). The shape of the transmission spectrum at the throughput port is Lorentzian shape. Mostly, these type of two ring resonators is used in filters [36] and [37]. Another way is to use different types of waveguide coupled configuration [38].

Parallel Coupled Two Ring Design

The illustration of a parallel coupled two-ring design is presented in figure 3. From this model, the fields in-ring waveguide can be calculated as follows:

$$E_{1a} = -k_1^* E_{i1} + t_1^* \alpha_1 e^{j\frac{\theta_1}{2}} E_{1b} \quad (10)$$

$$E_{1b} = t_2^* \alpha_1 e^{j\frac{\theta_1}{2}} E_{1a} - k_2^* e^{j\theta_w} (k_4 \alpha_2 e^{j\frac{\theta_2}{2}} E_{2a} - t_4 E_{i2}) \quad (11)$$

$$E_{2a} = -k_3^* e^{j\theta_w} (t_1 E_{i1} + k_1 \alpha_1 e^{j\frac{\theta_1}{2}} E_{1b}) + t_3^* \alpha_2 e^{j\frac{\theta_2}{2}} E_{2b} \quad (12)$$

$$E_{2b} = -k_4^* E_{i2} + t_4^* \alpha_2 e^{j\frac{\theta_2}{2}} E_{2a} \quad (13)$$

$$E_{t1} = t_1 e^{j\theta_w} (t_1 E_{i1} + k_1 \alpha_1 e^{j\frac{\theta_1}{2}} E_{1b}) + k_3 \alpha_2 e^{j\frac{\theta_2}{2}} E_{2b} \quad (14)$$

$$E_{t2} = t_2 e^{j\theta_w} (t_4 E_{i2} + k_4 \alpha_2 e^{j\frac{\theta_2}{2}} E_{2b}) + k_2 \alpha_1 e^{j\frac{\theta_1}{2}} E_{1a} \quad (15)$$

$$\theta_w = k_W \cdot n_{w_{eff}} \cdot \Lambda \quad (16)$$

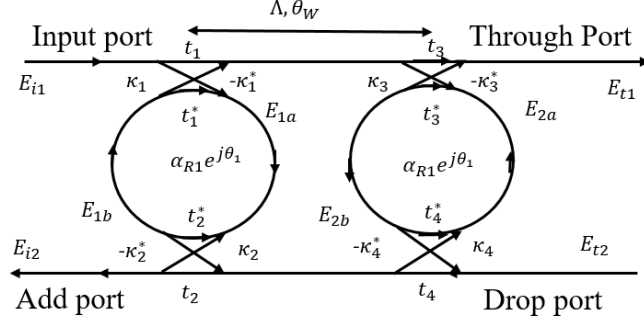


Figure 8 Electric fields in parallel-coupled two-ring design[1]

where θ_w is the phase shift, Λ is path length difference and $n_{W_{eff}}$ is an effective refractive index.

Using (10) to (16), one can derive the transfer function of the throughput and drop port. By considering the lossless couplers and waveguide, $t = t^*$ and $\kappa = -\kappa^*$, the amplitude forms for throughput port changes to zero. ($E_{i2} = 0$).

$$\frac{E_{t1}}{E_{i1}} = t_3 t_1 e^{j\theta_w} + t_3 k_1 \alpha_1 e^{j\theta_w \frac{\theta_1}{2}} \left[h + \frac{f(a+bc)}{1-d} \right] + k_3 t_4 \alpha_2^2 e^{j\theta_2} \frac{a+bc}{1-d} \quad (17)$$

And for the drop port:

$$\frac{E_{t2}}{E_{i1}} = k_1 k_2 \alpha_1 e^{j\frac{\theta_1}{2}} + k_2 t_1 \alpha_1^2 e^{j\theta_1} \left[h + \frac{f(a+bc)}{1-d} \right] + t_2 k_4 \alpha_2 e^{j\theta_w \frac{\theta_2}{2}} \frac{a+bc}{1-d} \quad (18)$$

The length of the waveguide can be changed to increase the overall FSR of this design. The reflected waves can be interfered constructively by choosing Λ in such a way that it should be an odd multiple $\frac{\lambda_0}{4}$.

$$\Lambda = (2m + 1) \frac{\lambda_0}{4n_{W_{eff}}} \quad (19)$$

One different form of parallel-coupled two-ring design is shown in figure 4, in which the gap between the ring waveguide is increased. The spectral transmission for this design has

been analyzed in [39]. A wavelength reflective filter can be designed by using four of the ring in a parallel manner[40].

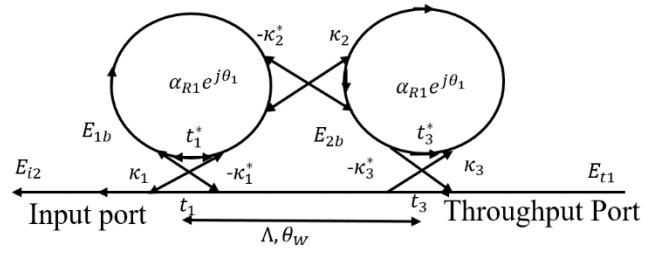


Figure 9. Special parallel-coupled two-ring design [1]

CHAPTER 3

DESIGN AND MODELING

In this chapter, the proposed optical ring resonator biosensor based on silicon photonics design and modeling is present. The overall system for biosensors consists of multi-wavelength laser, optical fiber, grating couplers, waveguides, ring resonator waveguide, coupling waveguide, and photodetector as shown in figure 10. In this section, the simulation results for the grating coupler, waveguide, and ring waveguide are presented along with the discussion on the complete ring resonator biosensor systems at the end. The simulations are performed in Lumerical MODE [41].

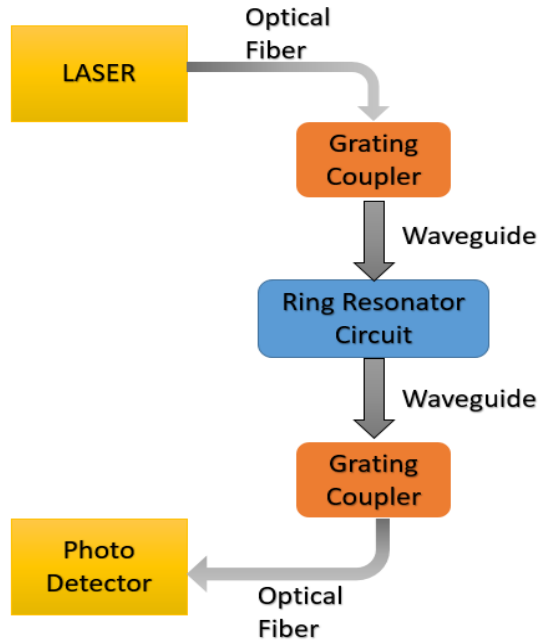


Figure 10 Proposed ring resonator bio sensor system

3.1 Grating Coupler

The cross-sectional area of an optical fiber core is almost 600 times larger than that of a silicon waveguide. Hence, we need components that adjust the mode field diameter accordingly. This is required to obtain efficient coupling from the fiber to the silicon chip and vice versa. The dimensions of our designed waveguide, discussed in the later section are 500x200 nm, which is very small as compared to the single-mode optical fiber whose diameter is 125 μ m. We used a surface grating coupler

as opposed to the edge coupling because edge coupling can only be used at the edge of the chip and the implementation of such design requires complicated post-processing and high-resolution optical alignment, which would increase the packaging cost. Grating couplers provide flexibility in the design and allow performing wafer or chip-scale automated testing. We have used Yan Wang [42] designed sub wavelength grating coupler optimized for a wavelength of 1550nm. The power reflection coefficients for the TE mode are -16.2dB and insertion loss of 4.1dB with 3dB bandwidth of 52.3nm, whereas for the TM mode the insertion loss is 3.74dB with a 3dB bandwidth of 82nm. The optimized sub-wavelength grating coupler for the TE₀₀ mode has a 593nm grating period, a 237nm grating width, and a 74nm sub-wavelength grating. The spectral response sub-wavelength grating coupler is shown in figure 11. The grating coupler is 127um apart because we are using a fiber array to probe the circuit for testing purpose.

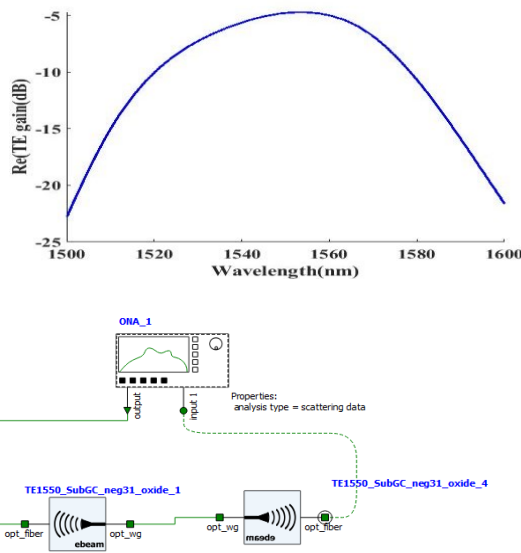


Figure 11 Spectral response for grating coupler and the grating coupler circuit with multi-wavelength laser, 127 um waveguide, and photodiode

3.2 Waveguide

A ring resonator is a circular shape waveguide. Therefore, we first performed the simulation in Lumerical MODE [41] for the waveguide and then used the same waveguide in a circular shape to

make a ring resonator. Here, we designed a strip waveguide with 500nm width and 220nm height using Lumerical MODE. The dimension of the integrated waveguide is shown in table I.

Table I Dimension of integrated waveguide

	Parameter	Dimension
SiO ₂	X	4um
	Y	4um
	Z	0.54um
Si	X	0.5um
	Y	0.22um
	Z	0.54um

We simulated the waveguide to calculate the effective index for the wavelength of 1550nm. Figure 13 shows the electric field intensity, figure 15 shows the magnetic field, and figure 14 shows the energy density for the TE₀ mode propagating in the designed optical waveguide. Figure 12 shows the screenshot taken from Lumerical MODE software.

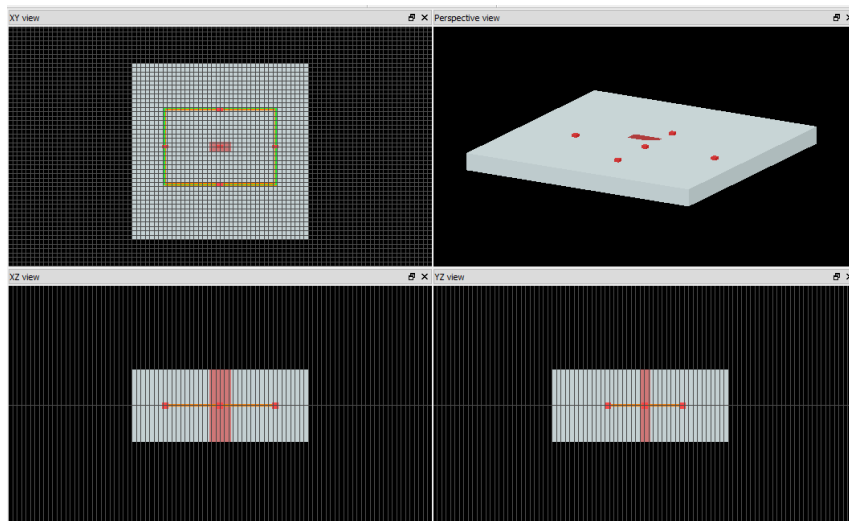


Figure 12 3D modeling of the integrated waveguide in Lumerical MODE.

The effective index can be modeled using the Taylor expansion around the center wavelength as shown in equation 1. Using the script editor of MODE we performed the curve fitting for n_{eff} for our design, which is shown in equation 2.

$$n_{eff}(\lambda) = n_1 + n_2(\lambda - \lambda_0) + n_3(\lambda - \lambda_0)^2 \quad (1)$$

$$n_{eff}(\lambda) = 2.44733 - 1.13268(\lambda - 1.55) - 0.0439436(\lambda - 1.55)^2 \quad (2)$$

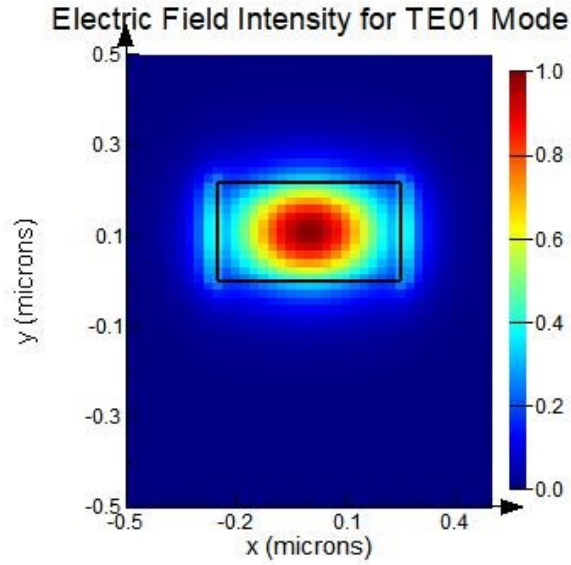


Figure 13 Electric Field Intensity for TE01 mode propagating in the waveguide

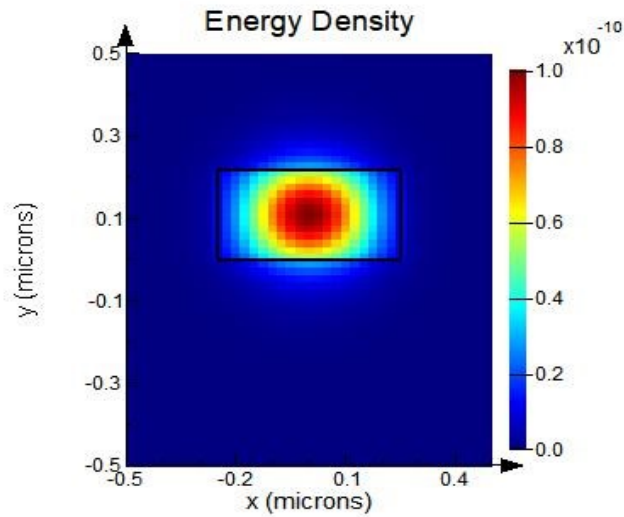


Figure 14 Energy density for TE02 mode propagating in the waveguide

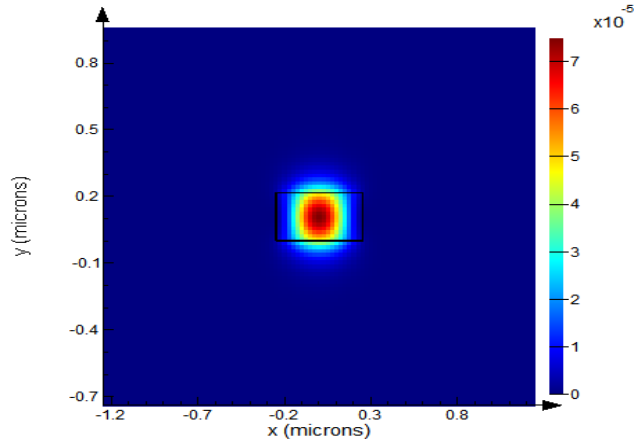


Figure 15 Magnetic Field Intensity for TE01 mode propagating in the waveguide

The results from this simulation give the S-parameters for waveguide, which is used in the Lumerical INTERCONNECT for ring resonator circuit design. When a waveguide is to bend as in our biosensor circuit, it induces an optical loss in terms of mode mismatch loss and radiation loss. If there is no optimized bend radius given to the waveguide, then significant scattering occurs at the transition from the straight region. This led to optical loss and multiple modes are excited by the bend. This phenomenon is shown in the figure for E-field with and without bending of the waveguide. However, in our designed ring resonator circuit, the optical light travels in fundamental mode as stated in the grating coupler discussion. Therefore, the model in the waveguide must be in fundamental mode. To understand the bend loss and mode mismatch, we analyzed the overlap function for the Eigen mode solver for the propagation of optical light in a waveguide with and without bent. After the overlap analysis with different bend radius, we concluded that the bend radius should be 5 μm for the TE mode, which is also the width of the waveguide, and 10 μm for the TM mode. Table II shows the loss percentage in overlap, which states that 5 μm radius for TE mode and 10 μm radius for bending waveguide give the least loss.

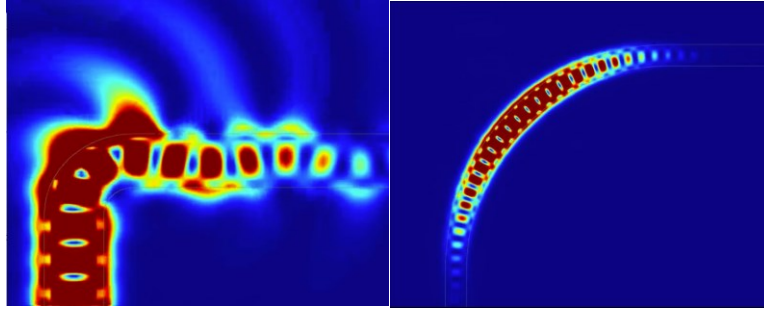


Figure 16 E-field without bending and with bending of the waveguide

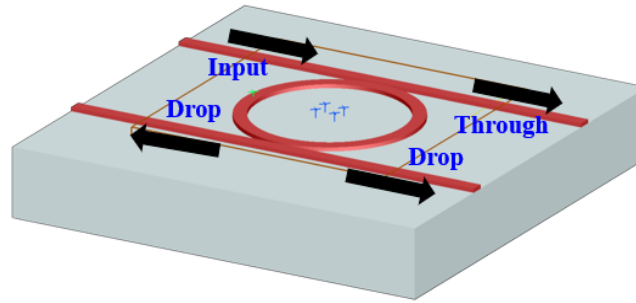
Table II Different bent radius overlap with the loss for TE and TM mode

Mode	Radius (μm)	Loss % in Overlap
TE	3	0.5
TE	4	0.28
TE	5	0.2
TM	5	10
TM	6	3.73
TM	10	0.73

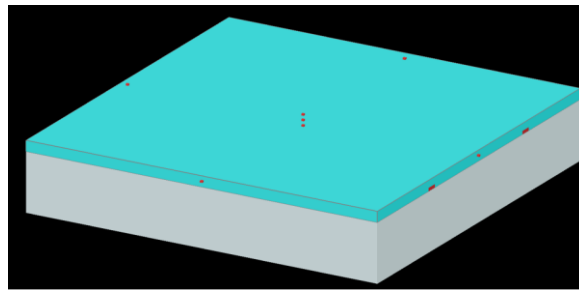
3.3 Ring Waveguide

A ring resonator is just a waveguide that is bent in a circular shape. Parameters for the proposed ring resonator are as follows: the radius of the ring (R) = $3.1\mu\text{m}$, the width of the ring (w_g) = 500nm , and the gap between the ring resonator and the waveguide (g) = 100nm . Table III presents the parameters for the ring resonator and the coupling waveguide.

(a)



(b)



(c)

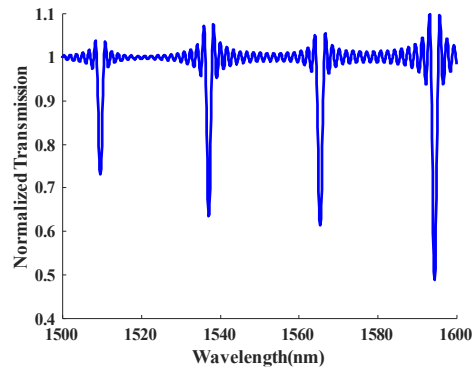


Figure 17 (a) 3D view for the ring resonator circuit showing the through and drop port, colored part is Si and grey part is SiO₂ (b) same ring resonator structure covered with known refractive index material and (c) Transmission spectra of ring resonator circuit at through port in Lumerical MODE

Table III Ring Resonator and coupling waveguide parameters

Parameter	Symbol	Value μm
Radius	R	3.1
Gap	g	0.1
Width of waveguide	wG	0.5
Thickness of waveguide	h	0.22

Figure 17 (a) shows the 3D view of the ring resonator circuit in Lumerical MODE and Figure 17 (b) shows the transmission spectra of the ring resonator. The same 3D structure was generated in COMSOL as shown in figure 18 (a) with its transmission spectra in figure 18 (b).

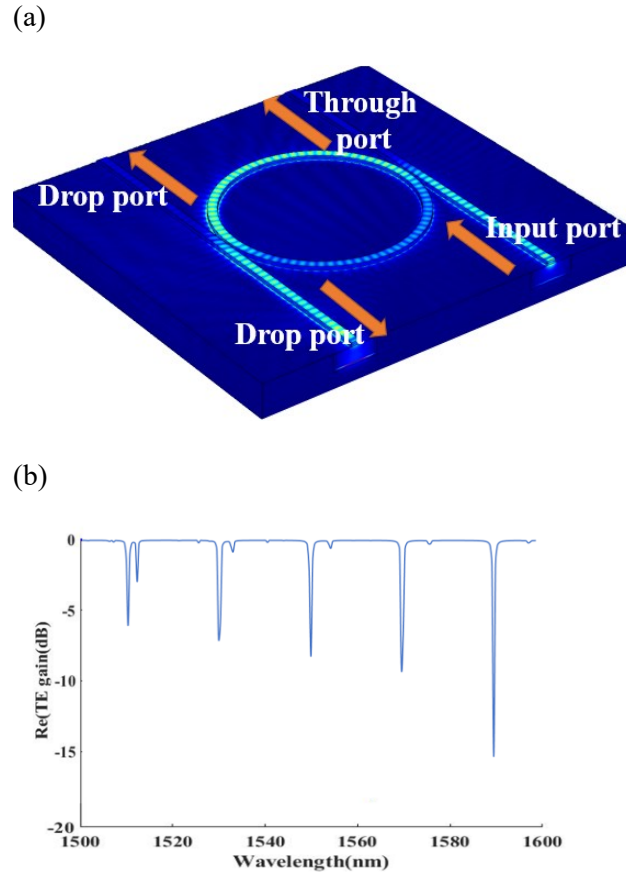


Figure 18 (a) 3D view for the ring resonator circuit with (b) Transmission spectra of ring resonator circuit through software COMSOL

3.4 Ring Resonator Biosensor System

As shown in figure 10 the ring resonator biosensor system consists of grating couplers, linear waveguide, and ring waveguide. We first designed and simulate the individual components and then combined all the components in Lumerical INTERCONNECT to design a complete biosensor system, which is shown in figure 19. The ring resonator circuit designed in this software contains the components from the library SiEPIC EBeam PDK[43] whereas figure 20 shows the spectral response for wavelength 1500nm to 1600nm. The response gives the minimum loss in transmission around the wavelength 1550nm. The reason is all the component in the circuit are optimized around wavelength 1550nm

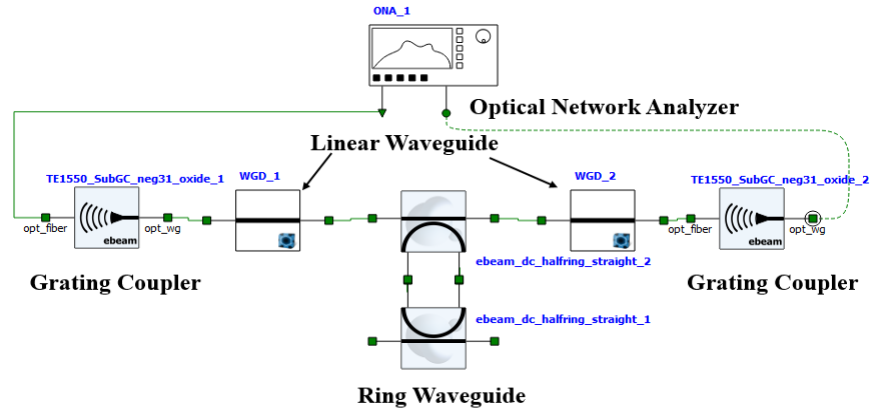


Figure 19 Ring Resonator Bio Sensor System in Lumerical INTERCONNECT

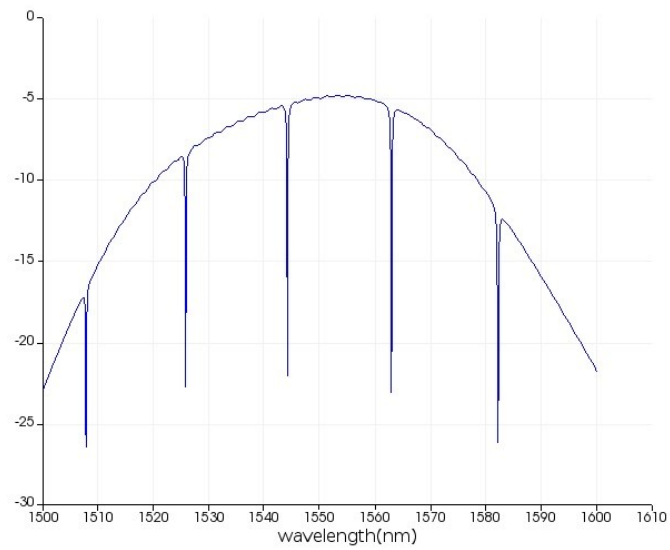


Figure 20 Spectral response of ring resonator circuit for wavelength 1500 to 1600nm

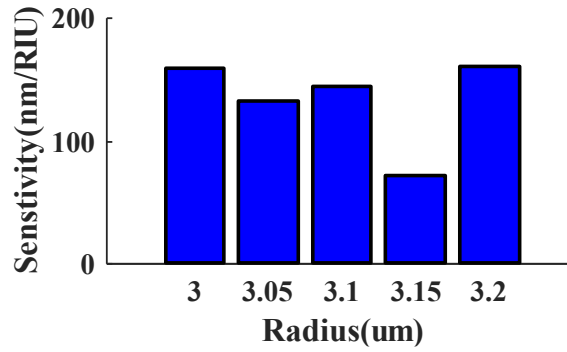
CHAPTER 4

BIOSENSOR COMPONENT OPTIMIZATION

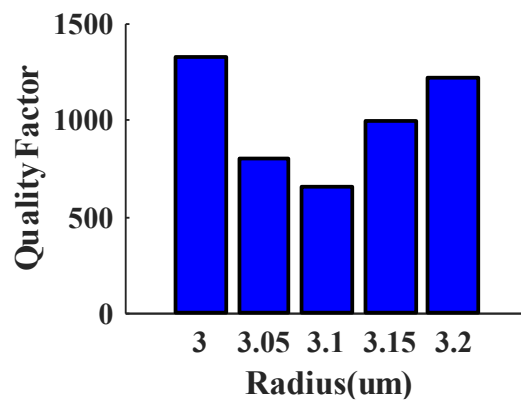
In this chapter, the proposed optical ring resonator biosensor components are optimized based on the quality factor and sensitivity. First, the radius of the ring waveguide is optimized, then the dimension of the waveguide is optimized for the highest quality factor and sensitivity. In all the processes of optimization, the condition of single-mode transmission and resonances is applied. To optimize the ring resonator for higher sensitivity and quality factors, the following analysis is performed.

4.1 Radii Analysis

The first analysis is performed to find out the optimized radius for the ring resonator by keeping other parameters for the ring resonator constant. For sensitivity calculation, the refractive index for the top layer of the ring resonator is set to $n=1$, and then it is changed to $n=1.1$. In this way, the difference of refractive index unit RIU and change in resonance wavelength are applied to equation (3) to calculate the sensitivity. Figure 21 shows the quality factor and sensitivity values for different radii of the ring resonator. The radii used in the simulation is from 3 μm to 3.2 μm with a difference of 0.05 μm . It can be observed from Figure 21 that radius 3 μm shows the maximum quality factor, whereas radius 3 and 3.2 show the maximum sensitivity. For further simulation, the radius of 3 μm is used because it shows the optimum quality factor and sensitivity.



(a)



(b)

Figure 21. Variation of (a) Sensitivity and (b) Quality factor with a change in radius of ring waveguide.

4.2 Waveguide Width and Height analysis

The next step is to increase the Q-factor without compromise the sensitivity of the proposed sensor. Further optimization is required to make the sensor highly accurate, efficient and it is done by placing pure blood on the ring resonator. The optimization procedure with measured optimization parameters is discussed in Table IV.

Table IV Optimization of the ring resonator, radius = $3\mu\text{m}$, and gap = $0.1\mu\text{m}$ and changing waveguide width and height

Waveguide width(μm)	Waveguide Height(μm)	Resonant Wavelength (μm)	Sensitivity	Quality Factor
0.4	0.18	No resonance	0	0
0.45		1.51866	229	1339.02
0.5		1.53485	158.3	1324.86
0.4	0.2	No resonance	0	0
0.45		1.51884	174	1316.53
0.5		1.53504	158.2	1324.73
0.4	0.22	No resonance	0	0
0.45		1.51899	173.9	1316.4
0.5		1.5352	158	1324.59

The first step of optimization is to change the width of the waveguide (wG) from $0.4\mu\text{m}$ to $0.5\mu\text{m}$ with an increment of $0.05\mu\text{m}$ while keeping the height of the waveguide as $0.22\mu\text{m}$. We found that at $wG = 0.45\mu\text{m}$ maximum value of sensitivity and quality factor occurs with 158 and 1324.59 respectively. It is further changing the height of the waveguide (h) from $0.18\mu\text{m}$ to $0.22\mu\text{m}$ with an increment of $0.02\mu\text{m}$ for all the values of the width of the waveguide. It is observed that at some combination for waveguide width and height there is no resonance as shown in table IV. Final values obtained after waveguide height and width for which the sensitivity and quality factor is maximum are $wG = 0.45\mu\text{m}$ and $h = 0.18\mu\text{m}$. All finalized steps are highlighted in table IV. During the simulation;

it is observed that the sensitivity and quality factor follows the opposite trend. In the proposed final structure, the parameters for the ring resonator are acceptable and reasonable for fabrication to perform a practical experiment on the ring resonator biosensor.

CHAPTER 5

ANALYSIS OF CANCER CELL

In this chapter, the proposed optical ring resonator biosensor is applied for biosensing application which is to detect cancer cells from the blood sample. First, the unoptimized ring resonator biosensor is applied then an optimized biosensor is applied, and in the end, the comparison is shown in form of the table to present the improvement in the biosensor system.

5.1 Refractive Index of Cancer Cell

Different blood samples have different permittivity (ϵ), and according to relation ($\epsilon = \eta^2$), the blood samples have a different refractive index. The refractive index of healthy person blood is 1.35 [44] whereas the refractive index of blood having a particular cancer cell is different as shown the table V. The propagation of light will vary in ring resonator with various samples of blood because of their different refractive indices. In the simulation, it is assumed that the refractive index of the mass covering the surface of the ring resonator is varied according to blood samples, and corresponding change at the output in transmission spectra is observed by simulation for five different cancer cell lines along with healthy person's blood sample as shown in Figure 22.

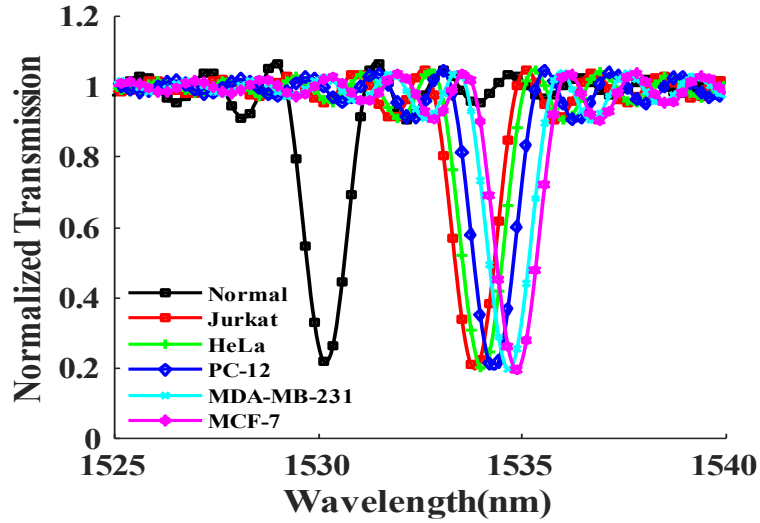


Figure 22. Transmission spectra for different cells along with their refractive indices. Parameters

for ring resonator $R = 3.1 \mu\text{m}$, $g = 0.1 \mu\text{m}$, $wG = 0.5 \mu\text{m}$, $h = 0.22 \mu\text{m}$

Table V Cancer cell line with their refractive index of the sample[2]

Name of Cell	Disease	Refractive index
Normal		1.35
Jurkat	Leukemia	1.39
HeLa	Cervical Cancer	1.392
PC-12	Brain	1.395
MDA-MB-231	Breast Cancer	1.399
MCF-7	Breast Cancer	1.401

5.2 Comparison of Unoptimized and Optimized

Results are shown for five different cancer cell lines including a normal blood sample, which can be easily differentiated from infected blood samples, but the peak for a different cancer blood sample is very close to each other with a minimum distance of 0.18nm. Other parameters to quantify the specific cancer cell line is a quality factor and sensitivity which are calculated according to equation (3)-(4) is very low as in the unoptimized column data analysis. To optimize the ring resonator for higher

sensitivity and quality factors, the following analysis is performed. The optimized structure is simulated for different cancer cell lines including the normal cell, and corresponding transmission spectra are shown in Figure 23. Variation for both measuring parameters sensitivity and quality factor for different cancer cells is shown in Table VI.

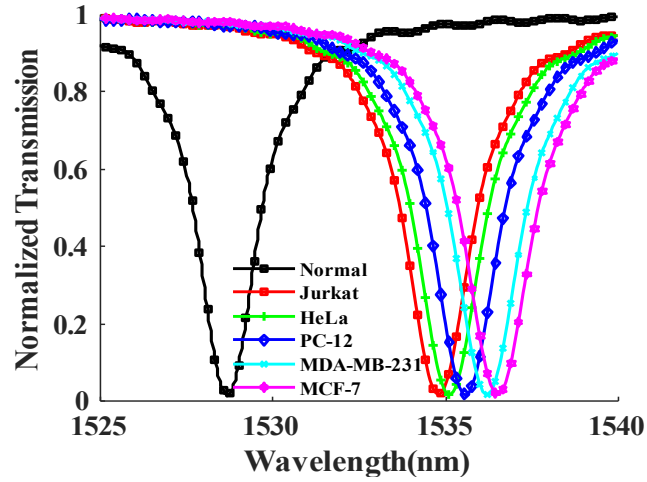


Figure 23. Transmission spectra for different cells along with their refractive indices for the optimized for ring resonator $R = 3 \mu\text{m}$, $g = 0.1 \mu\text{m}$, $wG = 0.45 \mu\text{m}$, $h = 0.18 \mu\text{m}$

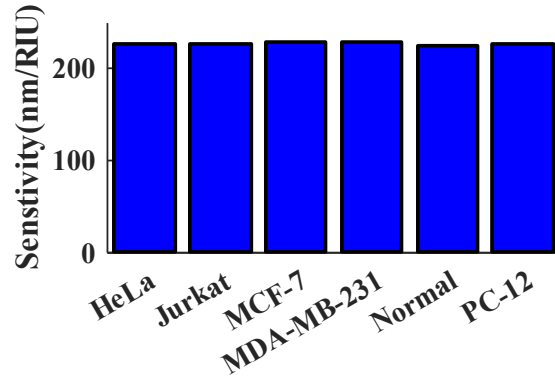
Table VI Resonance wavelength, quality factor, and sensitivity for normal and different cancer blood sample from an optimized ring resonator

Blood Sample	Unoptimized Ring Resonator			Optimized Ring Resonator			Improvement(%)	
	Resonant Wavelength (μm)	Quality Factor	Sensitivity	Resonant Wavelength (μm)	Quality Factor	Sensitivity	Quality Factor	Sensitivity
Normal	1.52982	554.98	191.857	1.52906	1386.45	223.41	59.97	14.12
Jurkat	1.53348	520.289	195.33	1.53272	1386.88	225.34	62.48	13.31
HeLa	1.53367	520.153	195.714	1.5329	1378.86	225.51	62.27	13.21
PC-12	1.53395	519.959	195.6	1.5332	1370.78	226.22	62.06	13.53
MDA-MB-231	1.53432	516.182	196.19	1.53357	1362.66	227.54	62.11	13.77
MCF-7	1.53451	516.05	196.31	1.53375	1354.98	226.71	61.91	13.40

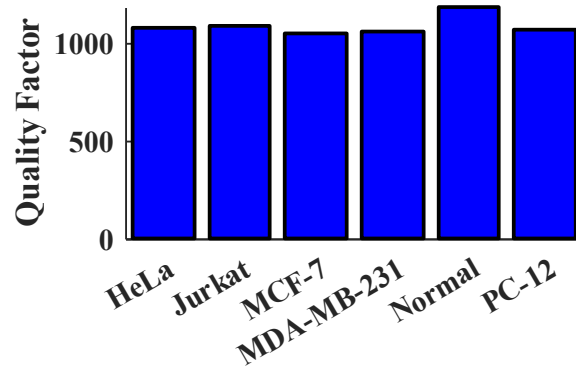
High sensitivity and quality factors are obtained as compared to unoptimized structure results. Figure 24 (a) and (b) shows the quality factor and sensitivity in the bar chart for the optimized ring resonator for a different disease blood sample. shows the comparison of our optimized biosensor with [2], although our proposed biosensor presents lower quality factor and sensitivity, the main advantage of our device is it is based on the integrated silicon photonics technology, which means the same CMOS foundry which fabricates integrated circuits can be used to fabricate the biosensor which will reduce the cost very low.

Table VII Comparison with other work

	Quality Factor	Sensitivity
S. Jindal [42]	4850	1150
Proposed Design	1380	225



(a)



(b)

Figure 24. Quality factor and Sensitivity for different cancer cells for optimized ring resonator circuit.

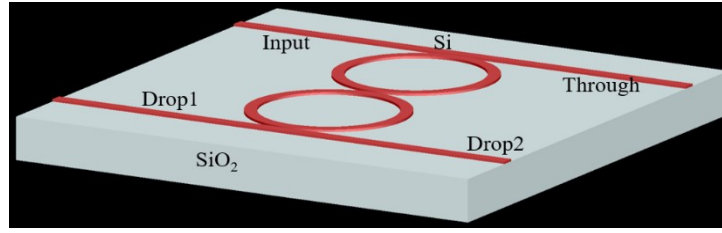
CHAPTER 6

TWO RING RESONATOR BIOSENSOR SYSTEM

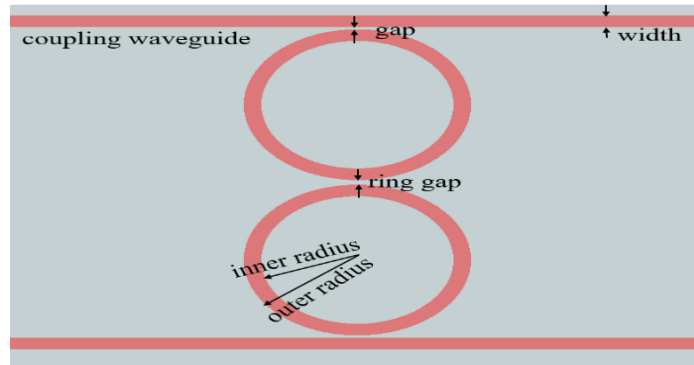
In this chapter, the proposed optical ring resonator biosensor components are optimized based on the quality factor and sensitivity. First, the radius of the ring waveguide is optimized, then the dimension of the waveguide is optimized for the highest quality factor and sensitivity. In all the processes of optimization, the condition of single-mode transmission and resonances is applied. The design parameters for different configurations of the cascaded ring resonator are presented. In the simulation, various properties of the ring resonator are analyzed. The fundamental properties are resonance wavelength, quality factor, sensitivity, and extinction ratio. The ring resonator structures have been modeled and simulated in Lumerical MODE [41]. In terms of materials selection, Silicon (Si) is used as the core material for the waveguide, silicon dioxide (SiO₂) is used as the cladding on the bottom surface, and material of known refractive index is used as the top surface. Here, the idea is to put different materials on the top surface of the ring resonator for generating the simulation data. Each of these materials would have a refractive index equal to the refractive index value of a particular diseased cell sample so that the change in optical behavior of the proposed structure can be observed and optimized to be used as a biosensor.

6.1 Serially Coupled Two Ring Design

The structural model of the serially coupled two-ring design is presented in Figure 25, which consists of two linear coupling waveguides and two ring resonators in series with each other. The width of the linear waveguide is 0.5 μm , and the height is 0.22 μm , and the height and width of the ring waveguide are the same. The four ports are input, though, drop-1 and drop-2. The optical light from the laser source is coupled to the integrated waveguide at the input port by the grating coupler. Then the optical light is coupled to the top ring by the top linear waveguide, and it gets coupled to the bottom ring waveguide after that. The spectral transmission is observed at the through the port.



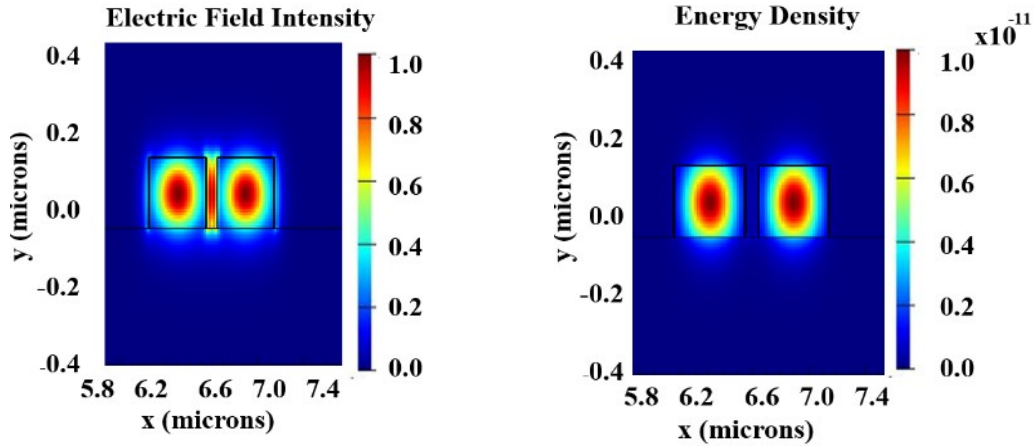
(a)



(b)

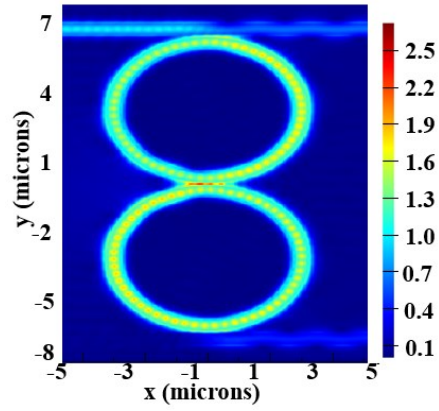
Figure 25. 3D view, red color material is Si, and grey color material is SiO₂ and (b) XY view of the serially coupled two ring resonator structure showing some parameters

In the serially coupled two-ring resonator, two ring waveguides are structured in top and bottom positions. To solve the optical mode inside the waveguide, the Eigenmode Solver method is applied at the point where the gap between the bus waveguide and the ring waveguide is minimum. The electric field intensity and the energy density for TE₀ mode propagating in the coupling waveguide and the upper ring waveguide are measured and shown in Figure 26.

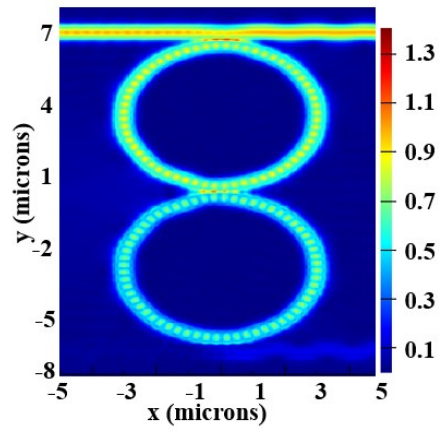


(a) (b)
 Figure 26. 3D Field Intensity and (b) Energy Density for TE₀ mode propagating in the waveguide

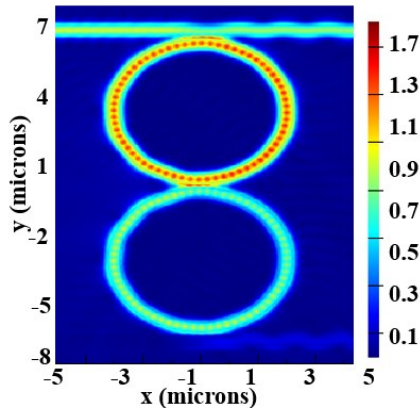
In this ring structure, the optical signal is transmitted from the input port, which gets coupled into the upper ring waveguide, and then coupled again to the lower ring waveguide. In figure 9, the coupling of light from the bus waveguide to the top ring waveguide and then two lower ring waveguides are observed. In Figure 27(a), light enters into the linear waveguide by input port, and it gets coupled to the upper ring, and then is coupled to the lower ring waveguide.



(a)



(b)



(c)

Figure 27. Coupling of light from linear waveguide to ring waveguide at (a) 1.5924 μm (b)1.56213 μm and (c)1.5019 μm

The spectral transmission for the range of wavelengths of 1.5 μm to 1.54 μm is shown in Figure 28. The serially coupled two-ring resonator shows a single dip resonance at 1.515 μm , whereas at

wavelength 1.535 μm , it shows two resonance dips. The quality factor is 721.85, sensitivity is 105, and the extinction ratio is -0.8765. The top surface of the ring circuit is not covered with any material.

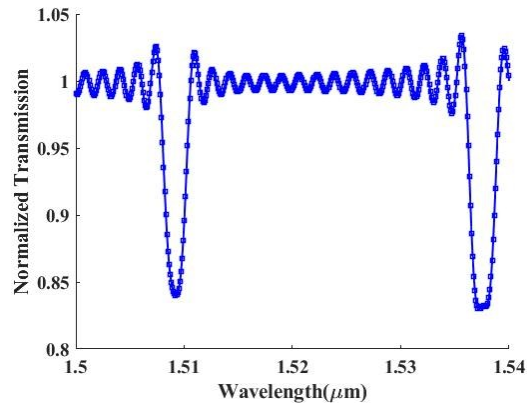


Figure 28. Spectral transmission on the through port for ring resonator circuit in figure 5(a).

6.2 Parallel Coupled Two Ring Design

In the parallel-coupled two-ring resonator, the ring waveguide is structured side by side with a 0.1 μm gap between the ring waveguide. To solve the optical mode inside the waveguide, the Eigenmode Solver method is applied at the point where the gap between the bus waveguide and the ring waveguide is minimum. The electric field intensity and the energy density for TE₀ mode propagating in the coupling waveguide and the upper ring waveguide are measured and shown in Figure 29 (a) and (b), respectively.

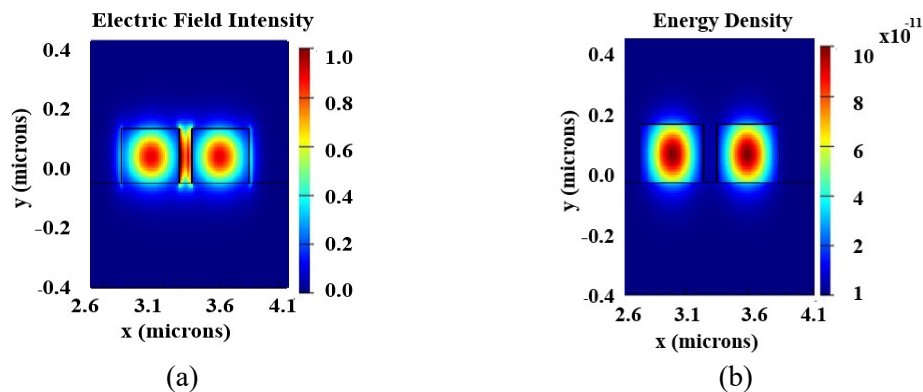


Figure 29(a) Electric Field Intensity and (b) Energy Density for TE₀ mode propagating in the waveguide

In this ring structure, the optical light can be coupled from two points from the bus waveguide, and also optical light can be coupled from one ring waveguide to another ring waveguide. Figure 30 shows the electric field intensity for different wavelengths. In Figure 30 (a), it can be observed that the optical light is not coupled into ring waveguide due to parameters of the ring waveguide, whereas in Figure 30 (b), the optical light is coupled to the first ring waveguide, and in Figure 30 (c) the optical light from the first ring waveguide is being coupled to the second ring waveguide.

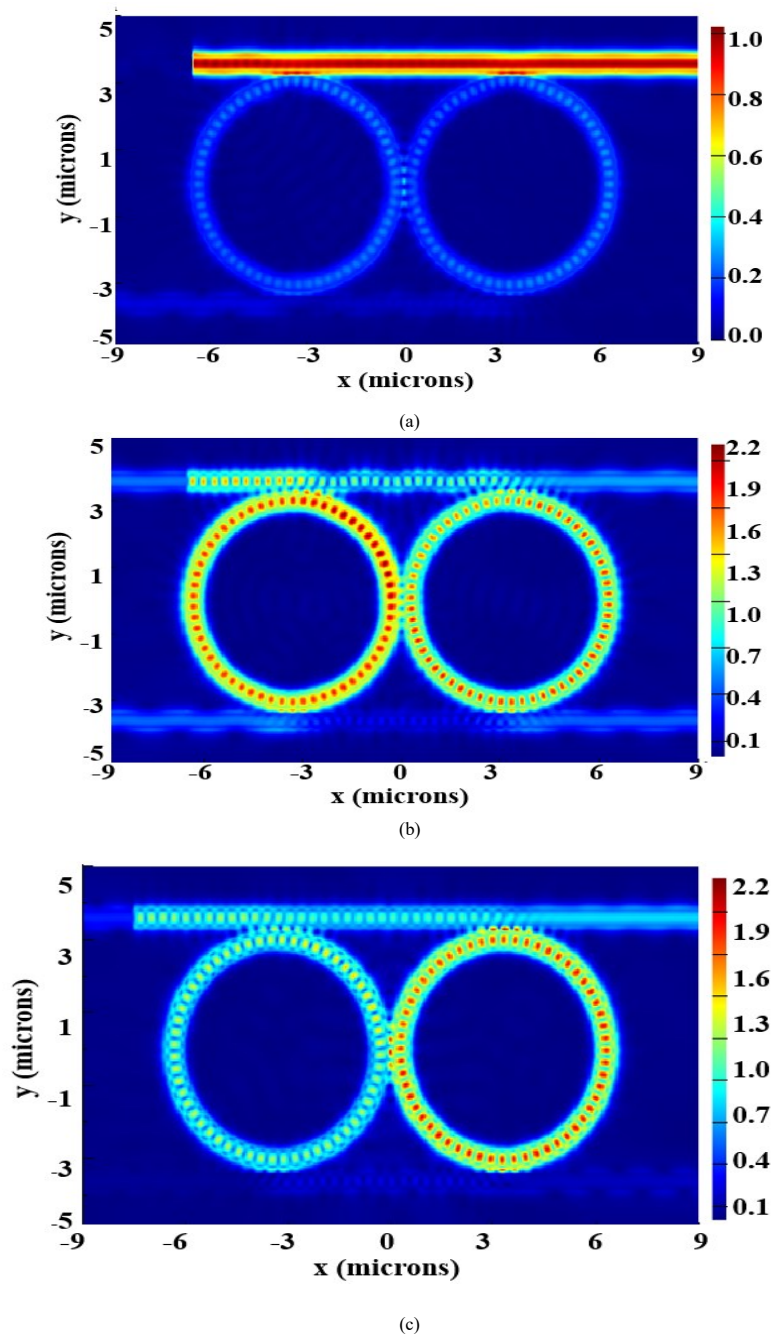


Figure 30 Coupling of light from linear waveguide to ring waveguide at (a) $1.5\mu\text{m}$ (b) $1.52015\mu\text{m}$ and (c) $1.59677\mu\text{m}$

The spectral transmission for the range of wavelengths of 1.5um to 1.54um is shown in Figure 31. It can be observed that the parallel-coupled two-ring resonator shows single dip resonance at 1.509 um and double-dip at 1.539. The top surface of the ring circuit is not covered with any material.

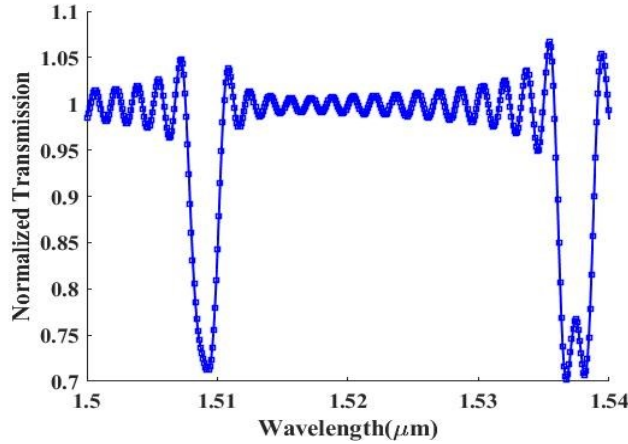


Figure 31 Spectral transmission on the through port for ring resonator circuit in figure 5(a).

The resonance wavelength, quality factor, sensitivity, and extinction ratio are 1.50931um, 685.364, 105, and -1.7536, respectively. The first analysis is performed to determine the optimized radius for both the ring resonator structures by keeping other parameters of the structure constant. The radius is varied from 3um to 3.2um. It has been observed that at the radius below 3um, the optical mode does not couple from bus waveguide to ring waveguide, and the reason for varying the radius to 3.2um is to keep the size of the resonator small as possible. Figure 21 shows the quality factor, and sensitivity for the radius varied from 3um to 3.2 for both serially and parallel-coupled two ring resonators. As shown in figure 21, radius 3.1um shows the maximum quality factor, sensitivity, and extinction ratio. In the subsequent section, the radius of 3.1um will be applied in the biosensor design.

6.3 Cascaded Ring Resonator as a Biosensor

Different blood samples have different permittivity (ϵ), and according to relation ($\epsilon = \eta^2$), the blood samples have a different refractive index. The refractive index of healthy person blood is 1.35 [44], whereas the refractive index of blood having a leukemia cancer cell is different, as shown in Table VIII.

Table VIII Refractive index of healthy blood and leukemia blood

Name of Cell	Disease	Refractive index	Antibody
Normal		1.35	
Jurkat	Leukemia	1.39[2]	Anti-CD-13[45]

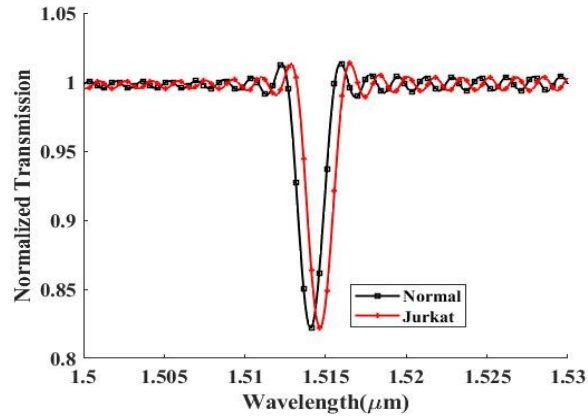
Figure 32 (a) shows the spectral transmission for a normal blood sample, which contains no cancer cell line, and (b) shows the blood sample containing the Jurkat cell, which shows the presence of leukemia for serially coupled and parallel-coupled two ring resonator respectively. Table IX shows the comparison for leukemia

Another way to detect the Jurkat cell in the blood sample is by the interaction of antibody and antigen, as shown in figure 15. Jurkat cell contains CD3+ T-Lymphocyte cells[29]. The anti-CD3 antibody can be placed on the surface of the ring resonator to detect the CD3+ cells. When the blood sample of a person having Jurkat cell is flown over the surface of the cascaded ring resonator configuration, the antigen and antibody will react, and the reaction will be reciprocated in the change of resonance wavelength.

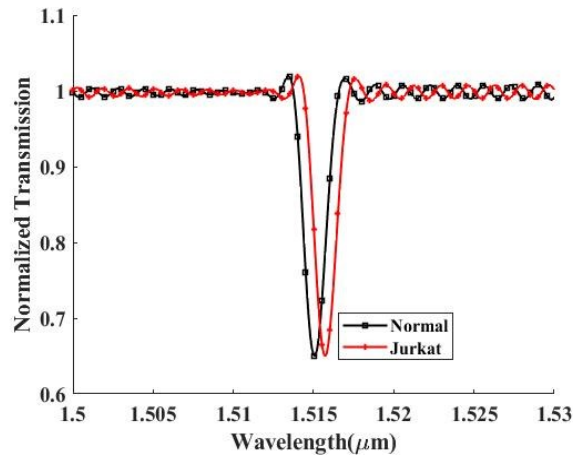
Table IX Quality factor and sensitivity for cascaded configuration

Configuration	Resonant wavelength (um)	Quality Factor	Sensitivity
Serially coupled two ring resonator	1.5152	890.7	120
Parallel coupled two ring resonator	1.5153	1001.5	201

Currently, the cytometer is used to precisely measure the CD3+ counts in a clinical manner[47]. This device in such a way that it counts the fluorescent signal by combine CD3+ cells with antibodies which has fluorescent property. Although these devices have high accuracy, they are expensive, require a trained specialist, and high upkeep requirements[47].



(a)



(b)

Figure 32 Spectral transmissions for a normal blood sample and Jurkat cell blood sample by (a) serially coupled and (b) parallel-coupled two ring resonators

The size of the Jurkat cell is $11.5 \pm 1.5\mu\text{m}$ [48], and for simulation purposes, one can consider the size of the anti-CD3 antibody similar. Both of the proposed cascaded ring configuration designs have the flexibility that the radius of the ring resonator could be changed to any value higher than $3\mu\text{m}$; as radius below $3\mu\text{m}$, there would be no coupling of optical mode between the bus waveguide and ring waveguide. For the antigen-antibody method of cancer detection, the radius of the ring resonator has been increased to $10\mu\text{m}$. Then the rectangular rod shape of the anti-CD3 antibody is placed on the surface of the ring resonator, as shown in Figure 34 (a) for serially and (b) for parallel-coupled two ring resonator.

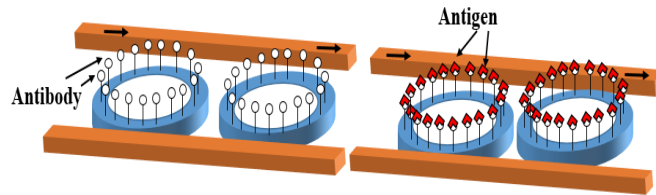
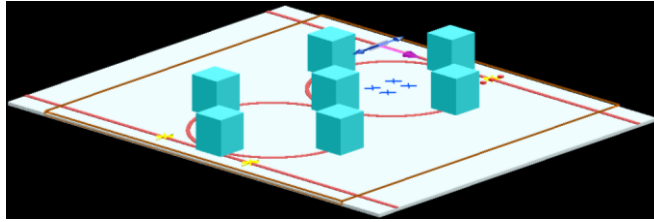
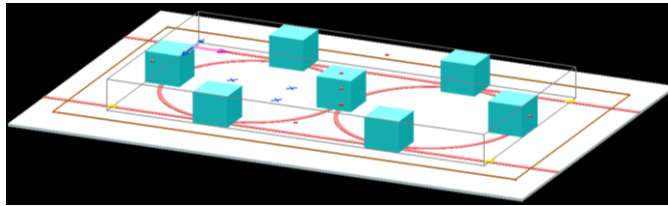


Figure 33 Proposed cascaded ring resonator circuit as a biosensor for the interaction of Antibody and Antigen

After placing the anti-CD3 antibody, the blood sample having a Jurkat cell is flown over the cascaded ring resonator. The antigen-antibody would react, and that change can be reciprocated in the shift in resonance wavelength, as shown in Figure 35. The rectangular bars are anti-CD3 antibody placed on the top surface of the ring resonator circuit as a biosensor for the interaction of Antibody and Antigen

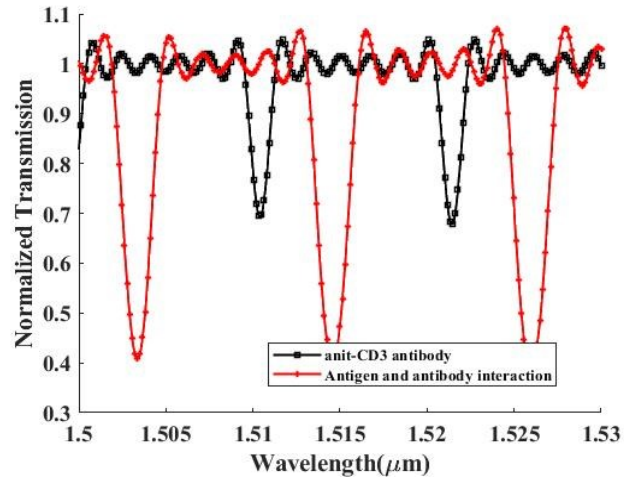


(a)

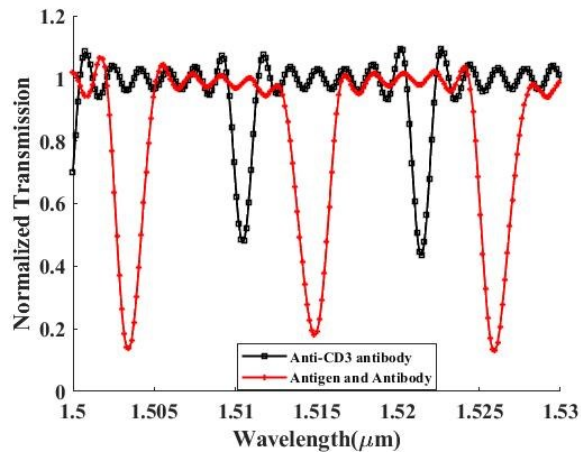


(b)

Figure 34. Proposed cascaded Proposed (a) serially and (b) parallel-coupled cascaded ring resonator for the interaction of Antibody and Antigen.



(a)



(b)

Figure 35. Spectral transmission after placing ant-CD3 antibody and after interaction of antigen-antibody on the surface of (a) serially and (b) parallel-coupled two ring resonator

CHAPTER 7

NON-INVASIVE MONITORING DEVICE FOR BRONCHIAL ASTHMA

In this chapter, we describe the process of applying a machine-learning algorithm to asthma data and generate a python flask application for monitoring the asthma attack for a patient. A research proposal was written for a non-invasive monitoring device for bronchial asthma by Dr. Mahrukh Khan and Dr. Masud Chowdhury for the NSF STTR proposal. Asthma is a chronic lung Disease, which involves people of all age groups. A lifelong disease causes wheezing, breathlessness, chest tightness, and coughing. It can limit a person's quality of life. According to the recent survey by Global Initiative for Asthma (GINA), the USA is among the few countries that have the worst numbers for prevalence of asthma in children aged 13-14 years. According to a Recent Survey by the Center for Disease Control (CDC), one in 13 people (about 24 million people) has asthma in 2016 in the USA. This situation is worse among children i.e. about 1 in 10 children (8.6%) had asthma in 2016. This alarming situation has increased medical and hospital costs with time. Asthma costs in the US grew from about \$53 billion in 2002 to about \$80 billion in 2013.

The goal of the project is to develop the necessary components of the communication technology to enable the deployment of patient-centric, portable and low-cost systems for the detection and monitoring of millions of people suffering from asthma. Deployment of noninvasive, low-cost patient-centric monitoring devices will help to reduce the costs of medical treatments. It will help the monitoring of patients especially children, who cannot perform specific maneuvers required in other monitoring systems of asthma. This non-invasive health monitoring system makes use of information collected due to scattering profiles between the sensors and affected bronchi in the lungs to provide continuous monitoring of the patient's condition during an asthma attack.

The physicians can make their decisions regarding the health and severity of the attack based on the analysis of this useful data. The operation and performance of this system are dependent hugely

on the efficiency of the antennas, making the antennas backbone of this health monitoring system. The block diagram for the asthma monitoring device is shown in Figure 36.

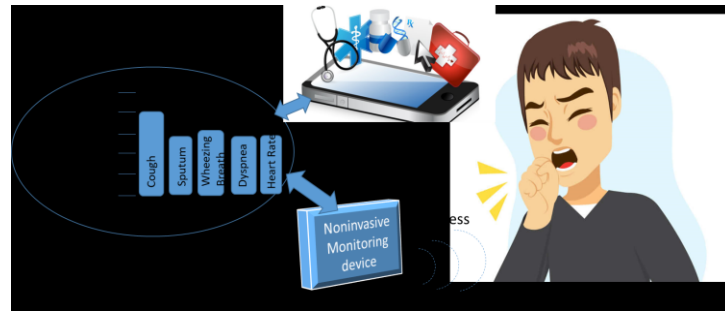


Figure 36 Non-invasive monitoring device for asthma

The proposed research work presents a potential solution of vital importance in providing efficient health monitoring for one of the most prevalent diseases in recent times. The proposed research work is anticipated to be accomplished in four phases. In the last phase of the project, when the Asthma data is received then a machine learning algorithm will be applied to the data to create a model and then this model will be used to detect the severity of the asthma attack.

7.1 Machine Learning Algorithm

For applying the machine learning algorithm, we have used the pycaret python library. This library does all processing apply different machine learning algorithm and then list the best algorithm with accuracy in a list form. Figure 37 shows the Python code.


```

1
2 from pycaret.utils import enable_colab
3 import pandas as pd
4 enable_colab()
5 dataset = pd.read_csv('asthma_data.csv')
6 dataset.shape
7 data = dataset.sample(frac=0.9, random_state=786)
8 data_unseen = dataset.drop(data.index)
9
10 data.reset_index(drop=True, inplace=True)
11 data_unseen.reset_index(drop=True, inplace=True)
12
13 print('Data for Modeling: ' + str(data.shape))
14 print('Unseen Data For Predictions: ' + str(data_unseen.shape))
15 from pycaret.classification import *
16 exp_mclf101 = setup(data = data, target = 'asthma_severity',
17                    session_id=123, normalize = True, polynomial_features = True, trigonometry_features = True,
18                    feature_interaction=True)
19
20 best = compare_models()
21
22 lr = best
23 tuned_lr = tune_model('lr')
24
25 final_lr = finalize_model(tuned_lr)

```

Figure 37 Python code for applying different machine learning algorithms on asthma dataset.

The code in line 5-7 load the dataset and then convert the dataset into a seen dataset which is going to be applied for machine learning and unseen dataset that we will use to measure the accuracy. Line 15-19 set up the pycaret library and then save the best machine learning algorithm. Line 23 tunes the algorithm to achieve more accuracy.

	Model	Accuracy	AUC	Recall	Prec.	F1	Kappa
0	Ridge Classifier	0.8950	0.0	0.8956	0.9010	0.8954	0.8425
1	Logistic Regression	0.8948	0.0	0.8956	0.9019	0.8956	0.8422
2	Random Forest Classifier	0.8922	0.0	0.8931	0.8981	0.8922	0.8384
3	Ada Boost Classifier	0.8921	0.0	0.8934	0.9003	0.8921	0.8382
4	Linear Discriminant Analysis	0.8920	0.0	0.8926	0.8981	0.8922	0.8380
5	K Neighbors Classifier	0.8918	0.0	0.8928	0.8985	0.8915	0.8377
6	Naive Bayes	0.8891	0.0	0.8898	0.8974	0.8901	0.8337
7	Extreme Gradient Boosting	0.8889	0.0	0.8892	0.8958	0.8893	0.8333
8	SVM - Linear Kernel	0.8862	0.0	0.8867	0.8919	0.8856	0.8292
9	Gradient Boosting Classifier	0.8860	0.0	0.8862	0.8937	0.8861	0.8290
10	Extra Trees Classifier	0.8831	0.0	0.8842	0.8946	0.8838	0.8247
11	Light Gradient Boosting Machine	0.8830	0.0	0.8832	0.8893	0.8833	0.8244
12	Decision Tree Classifier	0.8592	0.0	0.8602	0.8751	0.8604	0.7888
13	Quadratic Discriminant Analysis	0.6795	0.0	0.6751	0.6879	0.6202	0.5149

Figure 38 Comparison of a different machine learning algorithm for Asthma dataset

The model is saved and then load again to apply for one dataset to verify that the working of the model.

```
data_unseen1 = ['3', 'M', 'fds', '53', 'mild', 'wheezing', 'ert', '110']
cols = ['age', 'sex', 'color_of_skin', 'respiratory_rate', 'use_of_accessory_muscles', 'lung_auscultation', 'brain_function', 'heart_rate']
df_data_unseen_single = pd.DataFrame([data_unseen1], columns=cols)

new_prediction = predict_model(saved_final_lr, data=df_data_unseen_single)

if new_prediction.Label[0] == 0:
    print("Asthma is Mild")
elif new_prediction.Label[0] == 1:
    print("Asthma is Moderate")
else:
    print("Asthma is Severe")
```

Asthma is Severe

Figure 39 Machine learning model is applied for one row of asthma dataset

Further, I have written python code for the flask app so that it can be used by the health professional or it can be used in the future to constantly predict the asthma attack on a patient. The app can be transformed in such a way that whenever the asthma attack is severe a notification to the patient's physician and emergency contact can be sent for further investigation.

```
1 from flask import Flask, request, url_for, redirect, render_template, jsonify
2 from pycaret.regression import *
3 import pandas as pd
4 import pickle
5 import numpy as np
6
7 app = Flask(__name__)
8
9 model = load_model('Finallrmodel120Jan2021')
10
11 cols = ['age', 'sex', 'color_of_skin', 'respiratory_rate', 'use_of_accessory_muscles', 'lung_auscultation',
12 'brain_function', 'heart_rate']
13
14 @app.route('/')
15 def home():
16     return render_template("home.html")
17
18 @app.route('/predict', methods=['POST'])
19 def predict():
20     int_features = [x for x in request.form.values()]
21     print(int_features)
22     final = np.array(int_features)
23     data_unseen = pd.DataFrame([final], columns = cols)
24     prediction = predict_model(model, data=data_unseen, round = 0)
25     print(prediction)
26     prediction = prediction.Label[0]
27     if prediction==0:
28         prediction = 'Mild'
29     elif prediction == 1:
30         prediction = 'Moderate'
31     else:
32         prediction='Severe'
33
34     return render_template('home.html', pred='Curent Asthma is {}'.format(prediction))
35
36
37 if __name__ == '__main__':
38     app.run(debug=True)
39
```

Figure 40 Python for flask app for asthma monitoring

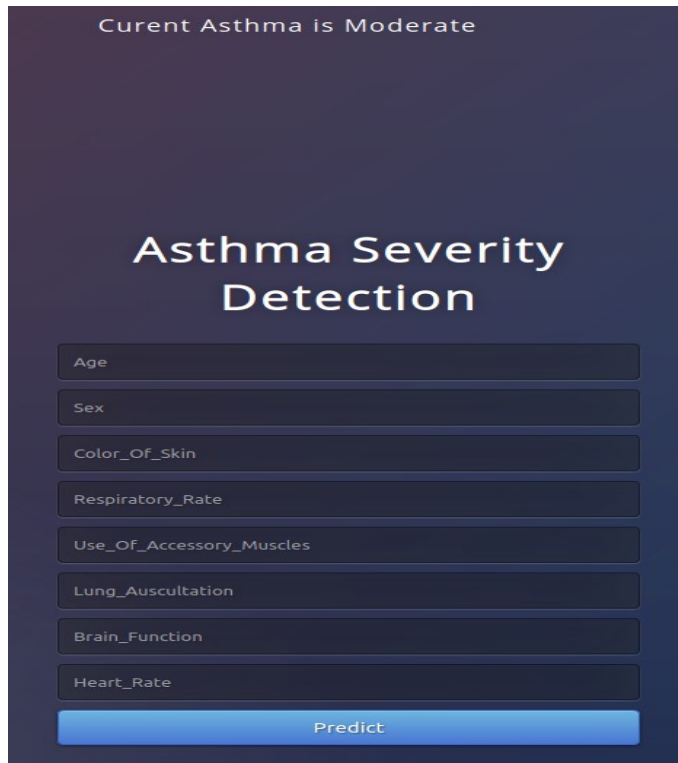


Figure 41 Python Flask app for Asthma severity detection.

CHAPTER 8

CONCLUSION & FUTURE WORK

8.1 Summary

In the first part of the Ph.D. thesis, a label-free ring resonator-based biosensing technique is proposed. The literature regarding the ring resonator biosensors is reviewed thoroughly then a novel biosensor based on silicon photonics ring resonator is proposed. The overall biosensing system consists of multi-wavelength laser, optical fiber, grating couplers, waveguides, ring resonator waveguide, coupling waveguide, and photodetector. For high sensitivity and selectivity, different designs of the ring resonators are simulated. Changes in the refractive index of the sample placed on the ring resonator surface lead to variation in the resonance wavelength of the ring resonator. This change can be used to identify the presence of cancerous cells in the blood sample. Further research can be performed to develop a biosensor that can quantify the cancer cells to detect the severity of cancer. The work is still at the theoretical stage, and we have focused on validating the concept through the numerical FDTD simulation of each of the components of the proposed biosensing system. In the future, we plan to fabricate the sensor using E-Beam Lithography technology, perform experiments for testing repeatability, linearity, and stability of the proposed biosensor, and compare the simulated and experimental results.

In the second part of the thesis, a label-free two-ring optical ring resonator-based biosensing technique has been proposed. The complete system consists of the following components: (i) laser generating wavelength from 1.5 μm to 1.6 μm , (ii) optical fiber to transmit optical light from the laser to the integrated coupling waveguide through the grating couplers, (iii) cascaded optical ring resonator configuration, and (iv) the photodetector. Two different designs of optical ring resonator in the cascaded setting is considered, which are the series and the parallel-coupled two ring resonator. The biosensor detects the cancer cell in the blood sample by observing the shift in the resonance wavelength because of the shift in the refractive index of the blood sample positioned on the top of the ring resonator. The

proposed biosensor has the potential to offer quick responses typically in two to three hours as compared to the available commercial cancer cell diagnosis methods, which take weeks. The size of the proposed sensor is in the millimeter range, which is a thousand times smaller compared to the traditional cancer sensors.

8.2 Future Work

This Ph.D. thesis focuses on analysis and simulation-based validation of the new biosensor design for detecting cancer cells. Before attempting any prototype development, there are many issues related to its performance and reliability that need to be resolved. As a direct extension, we would focus on adding new methodologies with the proposed design to quantify cancer cells using the cascaded ring configuration to be able to predict the stages of cancer. This new conceptual design of a cascaded optical ring resonator-based biosensor is analyzed using FDTD simulation of the Lumerical suite. The next step would be to fabricate a prototype using E-Beam Lithography. Optical ring resonators can be fabricated using the industry-standard CMOS process using silicon as the base material. Therefore, the commercial development of this type of sensor would be cost-effective, and it would be easy to integrate this sensor with the integrated bioelectronic circuits and systems. In the long run, we plan to partner with biomedical instrumentation and diagnosis research groups for clinical experimentation with real healthy and cancer-carrying blood samples to authenticate the simulated results.

REFERENCES

- [1] “Ring Resonators: Theory and Modeling,” in *Integrated Ring Resonators*, Springer, Berlin, Heidelberg, 2007, pp. 3–40. doi: 10.1007/978-3-540-68788-7_2.
- [2] S. Jindal, S. Sobti, M. Kumar, S. Sharma, and M. K. Pal, “Nanocavity-Coupled Photonic Crystal Waveguide as Highly Sensitive Platform for Cancer Detection,” *IEEE Sens. J.*, vol. 16, no. 10, pp. 3705–3710, May 2016, doi: 10.1109/JSEN.2016.2536105.
- [3] A. P. F. Turner, “Biosensors: Fundamentals and applications - Historic book now open access,” *Biosens. Bioelectron.*, vol. 65, p. A1, Mar. 2015, doi: 10.1016/j.bios.2014.10.027.
- [4] L. C. Clark and C. Lyons, “Electrode systems for continuous monitoring in cardiovascular surgery,” *Ann. N. Y. Acad. Sci.*, vol. 102, pp. 29–45, Oct. 1962.
- [5] M. C. Teich, *Fundamentals of Photonics*, 2 edition. Hoboken, N.J: Wiley-Interscience, 2007.
- [6] G. Carpintero, E. Garcia-Munoz, H. Hartnagel, S. Preu, and A. Raisanen, “Selected Emerging THz Technologies,” in *Semiconductor TeraHertz Technology: Devices and Systems at Room Temperature Operation*, Wiley-IEEE Press, 2015, pp. 408-. doi: 10.1002/9781118920411.ch8.
- [7] R. Soref, “The Past, Present, and Future of Silicon Photonics,” *IEEE J. Sel. Top. Quantum Electron.*, vol. 12, no. 6, pp. 1678–1687, Nov. 2006, doi: 10.1109/JSTQE.2006.883151.
- [8] L. Ali, M. Khan, M. U. Mohammed, A. H. B. Yousuf, and M. H. Chaudhry, “High Quality Silicon Photonics Optical Ring Resonator Biosensor Design,” in *2018 IEEE Nanotechnology Symposium (ANTS)*, Nov. 2018, pp. 1–3. doi: 10.1109/NANOTECH.2018.8653557.
- [9] K. Narsaiah, S. N. Jha, R. Bhardwaj, R. Sharma, and R. Kumar, “Optical biosensors for food quality and safety assurance—a review,” *J. Food Sci. Technol.*, vol. 49, no. 4, pp. 383–406, Aug. 2012, doi: 10.1007/s13197-011-0437-6.
- [10] F. Long, A. Zhu, and H. Shi, “Recent Advances in Optical Biosensors for Environmental Monitoring and Early Warning,” *Sensors*, vol. 13, no. 10, Art. no. 10, Oct. 2013, doi: 10.3390/s131013928.

- [11]M. U. Mohammed, A. Nizam, and M. H. Chowdhury, “Performance Stability Analysis of SRAM Cells Based on Different FinFET Devices in 7nm Technology,” in *2018 IEEE SOI-3D-Subthreshold Microelectronics Technology Unified Conference (S3S)*, Oct. 2018, pp. 1–3. doi: 10.1109/S3S.2018.8640161.
- [12]M. U. Mohammed and M. H. Chowdhury, “Reliability and Energy Efficiency of the Tunneling Transistor-Based 6T SRAM Cell in Sub-10 nm Domain,” *IEEE Trans. Circuits Syst. II Express Briefs*, vol. 65, no. 12, pp. 1829–1833, Dec. 2018, doi: 10.1109/TCSII.2018.2874897.
- [13]B. M. Paddle, “Biosensors for chemical and biological agents of defence interest,” *Biosens. Bioelectron.*, vol. 11, no. 11, pp. 1079–1113, Jan. 1996, doi: 10.1016/0956-5663(96)82333-5.
- [14]R. J. Essiambre, G. Kramer, P. J. Winzer, G. J. Foschini, and B. Goebel, “Capacity Limits of Optical Fiber Networks,” *J. Light. Technol.*, vol. 28, no. 4, pp. 662–701, Feb. 2010, doi: 10.1109/JLT.2009.2039464.
- [15]A. Yalcin *et al.*, “Optical sensing of biomolecules using microring resonators,” *IEEE J. Sel. Top. Quantum Electron.*, vol. 12, no. 1, pp. 148–155, Jan. 2006, doi: 10.1109/JSTQE.2005.863003.
- [16]J. Jágorská, H. Zhang, Z. Diao, N. L. Thomas, and R. Houdré, “Refractive index sensing with an air-slot photonic crystal nanocavity,” *Opt. Lett.*, vol. 35, no. 15, pp. 2523–2525, Aug. 2010, doi: 10.1364/OL.35.002523.
- [17]S. Yegnanarayanan, W. Roman, M. Soltani, G. Cremona, H. Lu, and A. Adibi, “On-chip Integration of Microfluidic Channels with Ultra-high Q Silicon Microdisk Resonators for Lab-on-a-Chip Sensing Applications,” in *LEOS 2007 - IEEE Lasers and Electro-Optics Society Annual Meeting Conference Proceedings*, Oct. 2007, pp. 50–51. doi: 10.1109/LEOS.2007.4382269.
- [18]P. Prabhathan, V. M. Murukeshan, Z. Jing, and P. V. Ramana, “Compact SOI nanowire refractive index sensor using phase shifted Bragg grating,” *Opt. Express*, vol. 17, no. 17, pp. 15330–15341, Aug. 2009, doi: 10.1364/OE.17.015330.

- [19]M. Iqbal *et al.*, “Label-Free Biosensor Arrays Based on Silicon Ring Resonators and High-Speed Optical Scanning Instrumentation,” *IEEE J. Sel. Top. Quantum Electron.*, vol. 16, no. 3, pp. 654–661, May 2010, doi: 10.1109/JSTQE.2009.2032510.
- [20]T. Claes, J. G. Molera, K. D. Vos, E. Schacht, R. Baets, and P. Bienstman, “Label-Free Biosensing With a Slot-Waveguide-Based Ring Resonator in Silicon on Insulator,” *IEEE Photonics J.*, vol. 1, no. 3, pp. 197–204, Sep. 2009, doi: 10.1109/JPHOT.2009.2031596.
- [21]Atlanta: American Cancer Society; 2017, “American Cancer Society, Cancer Prevention & Early Detection Facts & Figures 2017-2018.” [Online]. Available: <https://www.cancer.org/content/dam/cancer-org/research/cancer-facts-and-statistics/cancer-prevention-and-early-detection-facts-and-figures/cancer-prevention-and-early-detection-facts-and-figures-2017.pdf>
- [22]A. K. Sarkaleh, B. V. Lahijani, H. Saberhari, and A. Esmaeeli, “Optical Ring Resonators: A Platform for Biological Sensing Applications,” *J. Med. Signals Sens.*, vol. 7, no. 3, pp. 185–191, 2017.
- [23]M. E. Bosch, A. J. R. Sánchez, F. S. Rojas, and C. B. Ojeda, “Recent Development in Optical Fiber Biosensors,” *Sensors*, vol. 7, no. 6, pp. 797–859, Jun. 2007.
- [24]B. E. Little, J. P. Laine, and H. A. Haus, “Analytic theory of coupling from tapered fibers and half-blocks into microsphere resonators,” *J. Light. Technol.*, vol. 17, no. 4, pp. 704–715, Apr. 1999, doi: 10.1109/50.754802.
- [25]S. M. Grist *et al.*, “Silicon photonic micro-disk resonators for label-free biosensing,” *Opt. Express*, vol. 21, no. 7, pp. 7994–8006, Apr. 2013, doi: 10.1364/OE.21.007994.
- [26]B. Cai, S. Wang, L. Huang, Y. Ning, Z. Zhang, and G.-J. Zhang, “Ultrasensitive label-free detection of PNA-DNA hybridization by reduced graphene oxide field-effect transistor biosensor,” *ACS Nano*, vol. 8, no. 3, pp. 2632–2638, Mar. 2014, doi: 10.1021/nn4063424.

- [27]H. C. Engell, “Cancer cells in the circulating blood; a clinical study on the occurrence of cancer cells in the peripheral blood and in venous blood draining the tumour area at operation,” *Acta Chir. Scand. Suppl.*, vol. 201, pp. 1–70, 1955.
- [28]Z. Ruan, L. Shen, S. Zheng, and J. Wang, “Subwavelength grating slot (SWGS) waveguide on silicon platform,” *Opt. Express*, vol. 25, no. 15, pp. 18250–18264, Jul. 2017, doi: 10.1364/OE.25.018250.
- [29]K. Ogawa, W. Chang, B. Sopori, and F. Rosenbaum, “A theoretical analysis of etched grating couplers for integrated optics,” *IEEE J. Quantum Electron.*, vol. 9, no. 1, pp. 29–42, Jan. 1973, doi: 10.1109/JQE.1973.1077337.
- [30]O. Schwelb, “Transmission, group delay, and dispersion in single-ring optical resonators and add/drop filters—a tutorial overview,” *J. Light. Technol.*, vol. 22, no. 5, pp. 1380–1394, May 2004, doi: 10.1109/JLT.2004.827666.
- [31]W. Bogaerts *et al.*, “Silicon microring resonators,” *Laser Photonics Rev.*, vol. 6, no. 1, pp. 47–73, doi: 10.1002/lpor.201100017.
- [32]S. T. Chu, B. E. Little, W. Pan, T. Kaneko, S. Sato, and Y. Kokubun, “An eight-channel add-drop filter using vertically coupled microring resonators over a cross grid,” *IEEE Photonics Technol. Lett.*, vol. 11, no. 6, pp. 691–693, Jun. 1999, doi: 10.1109/68.766787.
- [33]S. J. Emelett and R. Soref, “Design and simulation of silicon microring optical routing switches,” *J. Light. Technol.*, vol. 23, no. 4, pp. 1800–1807, Apr. 2005, doi: 10.1109/JLT.2005.844494.
- [34]L. Ali, M. U. Mohammed, M. Khan, A. H. B. Yousuf, and M. H. Chowdhury, “High-Quality Optical Ring Resonator based Biosensor for Cancer Detection,” *IEEE Sens. J.*, pp. 1–1, 2019, doi: 10.1109/JSEN.2019.2950664.
- [35]B. E. Little, S. T. Chu, H. A. Haus, J. Foresi, and J.-P. Laine, “Microring resonator channel dropping filters,” *J. Light. Technol.*, vol. 15, no. 6, pp. 998–1005, Jun. 1997, doi: 10.1109/50.588673.

- [36]H. Suzuki, “Ring resonator device,” US5406238A, Apr. 11, 1995 Accessed: Nov. 14, 2019. [Online]. Available: <https://patents.google.com/patent/US5406238A/en>
- [37]M. Sorel, S. Gluck, and P. J. R. Laybourn, “Semiconductor double ring waveguide resonators,” *Electron. Lett.*, vol. 35, no. 18, pp. 1551–1552, Sep. 1999, doi: 10.1049/el:19991084.
- [38]I. S. Hidayat, Y. Toyota, O. Torigoe, O. Wada, and R. Koga, “Multipath structure for FSR expansion in waveguide-based optical ring resonator,” *Electron. Lett.*, vol. 39, no. 4, pp. 366–367, Feb. 2003, doi: 10.1049/el:20030276.
- [39]I. Chremmos and N. Uzunoglu, “Reflective properties of double-ring resonator system coupled to a waveguide,” *IEEE Photonics Technol. Lett.*, vol. 17, no. 10, pp. 2110–2112, Oct. 2005, doi: 10.1109/LPT.2005.854346.
- [40]J. K. S. Poon, J. Scheuer, Y. Xu, and A. Yariv, “Designing coupled-resonator optical waveguide delay lines,” *JOSA B*, vol. 21, no. 9, pp. 1665–1673, Sep. 2004, doi: 10.1364/JOSAB.21.001665.
- [41]MODE, *Lumerical*. Lumerical Inc. [Online]. Available: <https://www.lumerical.com/products/>
- [42]Y. Wang *et al.*, “Focusing sub-wavelength grating couplers with low back reflections for rapid prototyping of silicon photonic circuits,” *Opt. Express*, vol. 22, no. 17, pp. 20652–20662, Aug. 2014, doi: 10.1364/OE.22.020652.
- [43]L. Chrostowski *et al.*, “Design and simulation of silicon photonic schematics and layouts,” in *Silicon Photonics and Photonic Integrated Circuits V*, May 2016, vol. 9891, p. 989114. doi: 10.1117/12.2230376.
- [44]D. J. Rowe, D. Smith, and J. S. Wilkinson, “Complex refractive index spectra of whole blood and aqueous solutions of anticoagulants, analgesics and buffers in the mid-infrared,” *Sci. Rep.*, vol. 7, no. 1, p. 7356, Aug. 2017, doi: 10.1038/s41598-017-07842-0.
- [45]H. M. and H. M. et al, “Immunochemical Studies of an Antigen in a Human T-Cell Lymphoma Line (Jurkat) Recognized by Certain Monoclonal Antibodies to CD-13 (Aminopeptidase-N) | Kopernio.” <https://kopernio.com/viewer?doi=10.3109/10428199509056864&token=WzExNjc0MTMsIjEwL>

jMxMDkvMTA0MjgxOTk1MDkwNTY4NjQiXQ.c9DmZZTTSPc3bKswr96ryxpiEA8 (accessed Mar. 02, 2020).

- [46]N. Marano, D. Holowka, and B. Baird, “Bivalent binding of an anti-CD3 antibody to Jurkat cells induces association of the T cell receptor complex with the cytoskeleton,” *J. Immunol. Baltim. Md 1950*, vol. 143, no. 3, pp. 931–938, Aug. 1989.
- [47]K. Strauss *et al.*, “Performance evaluation of the FACSCount System: a dedicated system for clinical cellular analysis,” *Cytometry*, vol. 26, no. 1, pp. 52–59, Mar. 1996, doi: 10.1002/(SICI)1097-0320(19960315)26:1<52::AID-CYTO8>3.0.CO;2-I.
- [48]M. J. Rosenbluth, W. A. Lam, and D. A. Fletcher, “Force Microscopy of Nonadherent Cells: A Comparison of Leukemia Cell Deformability,” *Biophys. J.*, vol. 90, no. 8, pp. 2994–3003, Apr. 2006, doi: 10.1529/biophysj.105.067496.

VITA

Liaquat Ali received a B.S. degree in communication systems engineering from the Institute of Space Technology, Islamabad, Pakistan, in 2008. He has completed his M.S. degree in advanced optical technologies from Friedrich-Alexander-Universität Erlangen-Nürnberg, Germany. Currently, he is doing a Ph.D. at Computer Science Electrical Engineering Department, UMKC. Liaquat was awarded “UMKC School of Graduate Studies Research Grant, 2017.” His research interest includes Integrated Silicon Photonics circuits, Optical resonator, and biosensors, graphene-based biosensors, applying machine learning techniques in biosensors. He is serving as secretary at Graduate Student Council, UMKC. He has completed two internships, first as optical intern at Finisar Inc in year 2019 and second as testing development intern at Lumerical Inc in year 2020. He is student member of Optical Society America and IEEE.